NACA RM A55K21a

NACA

RESEARCH MEMORANDUM

FULL-SCALE WIND-TUNNEL TESTS OF THE LONGITUDINAL STABILITY AND CONTROL CHARACTERISTICS OF THE XV-1 CONVERTIPLANE IN THE AUTOROTATING FLIGHT RANGE

By David H. Hickey

Ames Aeronautical Laboratory
Moffett Field, Calif.

NATIONAL ADVISORY COMMITTEE
FOR AERONAUTICS

WASHINGTON

May 17, 1956

Declassified December 13, 1957

NATIONAL ADVISORY COMMITTEE FOR AERONAUTICS

RESEARCH MEMORANDUM

FULL-SCALE WIND-TUNNEL TESTS OF THE LONGITUDINAL STABILITY AND CONTROL CHARACTERISTICS OF THE XV-1 CONVERTIPLANE IN THE AUTOROTATING FLIGHT RANGE

By David H. Hickey

SUMMARY

An investigation was conducted to determine certain longitudinal stability, control, and performance characteristics of the XV-1 convertiplane in the autogiro- and airplane-type phases of flight. The fixed-wing and three-bladed rotor so share the total weight that in autogiro-type flight, the wing lift is small, whereas for airplane-type flight the rotor lift is small and constant.

In the autogiro-type flight configuration (speeds from 75 to 115 knots) the convertiplane was stable with speed, but was unstable with angle of attack. In the airplane-type flight range from 115 knots to maximum speed, stability both with speed and with angle of attack was noted. Adequate longitudinal control was indicated throughout the total airspeed range.

Interference between the fixed wing and rotor caused the lift-drag ratios of the complete aircraft to be appreciably less than the lift-drag ratios calculated from the individual component data.

Drag of the complete aircraft was reduced in a "clean-up" program. This reduction indicated an approximate 10-knot increase in maximum speed.

It is shown that reliable predictions can be made of the static stability contributions of the V-tab horizontal tail. Calculated downwash at the tail compared well with the measured downwash.

INTRODUCTION

The XV-1 convertiplane is designed to combine the features of a helicopter and an airplane. A helicopter-type rotor, a small fixed wing, and a pusher propeller are combined in an effort to obtain the best characteristics of both aircraft through the flight range from hovering to maximum forward speed.

The projected flight plan for the XV-1 convertiplane calls for: (1) helicopter flight from 0 to 80 knots forward speed, (2) transition (autogiro type) flight from 80 knots to 115 knots forward speed, and (3) airplane-type flight for forward speeds greater than 115 knots. In the transition speed range, autorotation of the rotor provides the major portion of the lift. At speeds above those for transition flight, the rotor lift is reduced to a small fraction of the total, although still in autorotation, so that the convertiplane characteristics are comparable to those of an airplane.

To enable accomplishment of flight in the transition range and airplane range, the XV-1 incorporates two novel features. The first of these is a floating horizontal stabilizer to minimize the adverse effect on longitudinal stability of the large downwash changes associated with the unusually broad speed range. The second is a control mechanism to allow stable rotor operation at high tip-speed ratios. Although small-scale model tests had been carried out to develop the various components of the aircraft and to show that their combination would enable accomplishment of the flight plan, a question existed as to the applicability of small-model data to the full-scale convertiplane in the transition and airplane phases of flight. Therefore, a full-scale wind-tunnel investigation was conducted in the Ames 40- by 80-foot wind tunnel in order to substantiate the integrity of the XV-1 design.

The principal purpose of this report is the determination of longitudinal stability, control, and performance characteristics of the convertiplane in the two autorotative conditions. In addition, certain relevant data affecting these characteristics are compared with other data obtained in the development tests. These data are presented in references 1 and 2. Furthermore, an analytical method is derived to estimate the V-tab horizontal-tail contribution to these characteristics and is compared to the full-scale and small model test results. Part of this analysis is presented in appendix B of reference 1. Some full scale, dynamic, and loads data for this convertiplane are presented in reference 3.

SYMBOLS

a	lift-curve slope, per deg
c	chord, ft

$\bar{c}$ mean aerodynamic chord (M.A.C.), $\dfrac{\int_0^{b/2} c^2 dy}{\int_0^{b/2} c\, dy}$, ft

C_D drag coefficient, $\dfrac{\text{drag}}{qS_R}$

C_L lift coefficient, $\dfrac{\text{lift}}{qS_R}$

C_m pitching-moment coefficient about the rearmost center-of-gravity position, $\dfrac{\text{pitching moment}}{qS_R R}$

C_{m_T} horizontal-tail pitching-moment coefficient about the hinge line, $\dfrac{\text{pitching moment}}{qS_T c_T}$

C_h hinge-moment coefficient, $\dfrac{\text{hinge moment}}{qS_t c_t}$

C_{h_δ} change in tab hinge-moment coefficient with respect to tab deflection, per deg

C_{h_α} change in tab hinge-moment coefficient with respect to the tail angle of attack, per deg

C_T rotor thrust coefficient, $\dfrac{T}{\rho(\omega R)^2 S_R}$

K trim-tab spring constant, ft-lb/deg

l_T distance from moment center to floating-tail hinge line, ft

q free-stream dynamic pressure, lb/sq ft

R rotor radius, ft

S area, sq ft

T resultant thrust of rotor, lb

w vertical component of velocity at any point in the rotor flow field, ft/sec

v free-stream air velocity, ft/sec

V free-stream air velocity, knots

α angle of attack, deg

α_f angle of attack of the propeller thrust axis with respect to the free stream, deg

β control stick deflection from center, deg

γ $\frac{\delta_t}{\delta_T}$, ratio of trim-tab deflection at some airspeed to trim-tab deflection at $q_T = 0$

$\Delta\alpha_f$ change in angle of attack, deg

$\Delta\delta_{ST}$ change in stabilizer incidence angle, deg

ΔC_m pitching-moment coefficient increment

ΔC_D drag coefficient increment

δ_S servo-tab angle with respect to the stabilizer chord line, deg

δ_{S_o} servo-tab setting (tab deflection at 0^o stabilizer angle), deg

δ_t trim-tab angle with respect to the stabilizer chord line, deg

δ_T trim-tab angle with respect to the stabilizer chord line at zero q_T, deg

δ_{T_o} trim-tab setting at zero q_T and zero stabilizer angle, deg

δ_{ST} stabilizer angle with respect to the thrust axis, deg

ϵ downwash angle, deg

μ tip speed ratio, $\frac{V}{\omega R}$

ρ density of free-stream air, slugs/cu ft

τ linkage ratio, change in tab deflection with change in stabilizer angle

ω angular velocity of rotor, radians/sec

Subscripts

R rotor

S servo tab

T horizontal tail

t trim tab

w wing

AIRCRAFT AND APPARATUS

Photographs of the XV-1 convertiplane as mounted in the test section of the wind tunnel are shown in figure 1. The geometric characteristics of the aircraft are given in figure 2 and table I.

Power Plant

The aircraft was powered by a 550-horsepower, nine-cylinder, radial engine. The power from the engine was used either for driving the rotor in helicopter flight or for driving the fixed-pitch, pusher-type propeller in autogiro-type and airplane-type flight. The function of the engine for helicopter flight was to drive two centrifugal air compressors that supplied air to the pressure jet engines on the rotor tips. Since helicopter flight was not studied in these tests, the burners were not operated. A brake was provided to lock the propeller during helicopter flight.

Rotor

The mechanics and characteristics of the convertiplane rotor hub and controls were essentially as described and discussed in references 2 and 4. A linkage was incorporated between the rotor blades and the swash plate which caused the actual blade pitch angle to depend on the coning angle (component of the blade flapping angle that is independent of rotor blade azimuth). One degree of positive coning angle reduced the blade pitch angle by 2.2°.

In the autogiro-type flight range, the incidence of the swash plate was fixed at $+3^{\circ}$, and the blade pitch angle at 0.75R was fixed at 6° (measured at zero coning angle) with reference to the swash plate. Changes in lift coefficient of the rotor were brought about by variation of angle of attack of the convertiplane.

In the airplane-type flight configuration, the hub was mechanically locked to the swash plate, and the blade pitch angle at 0.75R with respect to the swash plate was fixed at 0°. A governor was employed to tilt the swash plate in such a way as to keep the rotor rpm constant. In this configuration, the rotor-blade-swash-plate linkage minimized blade flapping motions, thus delaying blade flapping instability at the high advance ratios typical of the airplane-type flight configuration. Characteristics of the rotor were then as follows: (1) small rotor lift coefficient, (2) rotor lift coefficient constant with convertiplane angle of attack, and (3) rotor lift constant with airspeed.

Horizontal Tail

The XV-1 was equipped with a free-floating horizontal tail (designated V-tab horizontal tail) in order to alleviate the stability problems arising from the large variation of downwash encountered throughout the speed range. The tail and the linkage of the tabs to the controls are illustrated in figure 3. Location of the hinge line of the horizontal tail was at 22-1/2-percent chord. Two 15-percent-chord tabs, each half of the tail span, served as a trim tab and a servo tab. The trim tab on the XV-1 did not bring about zero stick force, but rather allowed positioning of the control column. An adjustable centering spring on the control column was used to obtain zero stick force. Another spring was placed in the trim-tab linkage to compensate partially for the change in downwash angle with forward speed. Downwash effects on the horizontal tail at forward speeds from 0 to 40 knots were minimized by a third spring which held the stabilizer at 60° deflection. The moment provided by the stabilizer spring is shown in figure 4(a). Both tabs were equipped with a linkage which provided an approximate sine curve relationship between the stabilizer angle and tab angles (fig. 4(b)). In the practical range of stabilizer angles, the linkage ratio was very nearly unity.

For the tests the horizontal tail was equipped with selsyn units to measure angles on the tabs and stabilizer. The tail lift was indicated by calibrated strain gages on the surfaces of the twin tail booms.

TESTS

The airspeed range of the tests conducted in the Ames 40- by 80-foot wind tunnel was from 75 to 150 knots.

The investigation consisted of five phases:

1. Tests to determine the convertiplane longitudinal characteristics and the V-tab horizontal-tail characteristics with the rotor blades and propeller removed.

2. Tests to determine the effect of the powered propeller on the convertiplane longitudinal characteristics and V-tab horizontal-tail characteristics with the rotor blades removed.

3. Tests to determine the con ertiplane longitudinal characteristics in both flight configurat ons with the propeller removed.

4. Tests to determine the effect of the powered propeller on the convertiplane longitudinal characteristics in both flight configurations.

5. Tests to determine the drag of the convertiplane components and means of reducing the drag. Figure 5 shows some of the pylon modifications tested during this phase of the investigation.

During the powered-propeller tests, it was necessary in some cases to allow pitch freedom above test airspeeds of 75 knots because otherwise the convertiplane developed undesirable vibrations. Pitch freedom was restricted to a total of $1/2^{\circ}$ in the autogiro-type flight configuration and 6° in the airplane-type flight configuration.

CORRECTIONS TO DATA

Strut drag tares were applied only to the data obtained in the studies of drag reduction. The drag tare of the pitch strut was obtained by removing the pitch strut and its fairings from the wind-tunnel test section, allowing the aircraft to float free. The change in drag due to the removal of the pitch strut was within the least count of the drag-indicating system. Drag of the main support struts was obtained after the convertiplane was removed from the test section and fairings were added to the strut ball sockets. A value of ΔC_D of 0.0006 was obtained for the main struts alone throughout the speed range investigated.

The least counts of the force coefficients when the convertiplane was restrained in pitch are shown below:

Quantity	Least count
Lift coefficient	±0.001
Tail lift coefficient	±.005
Drag coefficient	±.0001
Pitching-moment coefficient	±.0003

The least counts of all angular data, excepting δ_t, were ±0.25° with the aircraft fixed in pitch. The least count in δ_t data was about ±0.5°.

The least counts of force and angular data obtained during the free-to-pitch portion of the testing were increased, as shown below:

Quantity	Least count
Lift coefficient	±0.005
Tail lift coefficient	±.01
Drag coefficient	±.0002

The least counts of all the angular data with pitch freedom were about ±1°.

Boundary corrections were not applied for the convertiplane because they were unknown; however, wind-tunnel wall corrections to the data with rotor blades removed were calculated and found to be negligible.

PRESENTATION OF FIGURES

Full-Scale Data

These full-scale tests of the XV-1 convertiplane were directed toward an examination of only the autogiro-type and airplane-type flight configurations because the helicopter characteristics could be obtained relatively safely and easily in flight tests.

The three-component force data presented in figures 6 and 7 apply to the aircraft with rotor blades and propeller removed. These tests had the following purposes: (1) to determine the characteristics of the horizontal tail, (2) to serve as a basis for examining the effect on stability and control of adding a rotor to an airplane configuration, and (3) to serve as a basis for examining the effect on stability and control of adding the propeller slipstream.

The three-component force data presented in figures 8, 9, and 10 show the aircraft characteristics with the propeller removed in the autogiro-type and airplane-type flight regimes. These data are the basis for the stability and control analysis and performance evaluation presented herein.

The force data presented in figure 11 and table II are the results with power applied to the propeller with the rotor blades removed and are also utilized in the stability and control analysis.

The strain-gage and selsyn data presented in figures 12, 13, and 14 show the characteristics of the V-tab horizontal tail.

Figure 15 presents the measured downwash angles at the tail with and without the rotor. Calculated downwash angles at the tail in the autogiro-type flight configuration are also included for comparison.

The pitching-moment data presented in figure 16 are cross plots of the data presented in figure 7. These data are presented in this form to show the speed stability characteristics of the convertiplane without rotor blades.

Figure 17 presents force data showing the effect of rotor operation on the pitching-moment variation with airspeed. These data were obtained from the data presented in figures 8 and 10 for the propeller-removed configuration. The corresponding powered-propeller data at a trim-tab setting of -20° were those presented in table III. Only the data from the tests with the convertiplane fixed in pitch are presented in figure 17. In addition, the calculated variation of pitching moment with airspeed for powered-propeller conditions at a trim-tab setting of -60° is shown. Figure 17 is concluded with calculated curves, corresponding to the pitching-moment curves, showing the variation of stick position for trim with airspeed. These data were used to appraise the stick-motion stability of the convertiplane.

Figure 18 presents calculated values showing the control effectiveness of the V-tab horizontal tail. These results were used in the calculations performed to obtain the curves in figure 17.

Figures 19 and 20 present force data showing the effect on lift and drag of the combination of a fixed-wing and rotor for both convertiplane configurations considered. The data presented in figure 21 show the apparent decrease in the wing angle of attack when the wing is submerged in the rotor flow field. These data provide an estimate of the lift interference between a fixed wing and a rotor in combination.

Figure 22 presents data showing sea-level maximum speed and the increase in maximum speed realized by certain drag reductions. These data

were derived from the fixed-pitch force data in table III and the data shown in figures 8 and 10.

Small-Scale Tests

The results of certain tests with the small models used to develop the convertiplane are presented herein in order to assess their value in predicting the behavior of the full-scale machine. Although small-model tests are not strictly comparable to the full-scale tests, their use in respect to convertiplane design and development is general, and an indication of their reliability is therefore believed to be of value. Because an evaluation of the small-model data is not relevant to the principal purpose of this report, the data are included without discussion. All of the small model data were obtained from reference 1.

Test results presented herein were obtained as follows:

1. Rotor-blades, tail, rotor hub, and propeller-removed data were obtained from an 8/31-scale model of the XV-1 tested in the University of Washington 8- by 12-foot wind tunnel. Engine inlets, landing skids, wing-tip skids, and tail fans were not reproduced on the model. These data are presented in figure 6.

2. V-tab horizontal-tail data were obtained from test results of a geometrically and dynamically similar 2/5-scale model of the tail. The wing and fuselage tested in conjunction with the tail provided a downwash distribution similar to that expected for the full-scale convertiplane in airplane-type flight. The tests were conducted in the University of Washington 8- by 12-foot wind tunnel. These data are presented in figure 14.

3. Downwash angle at the tail was measured with a complete 8/31-scale model. The model was mounted in the return passage of the Wright Air Development Center 20-foot wind tunnel. The diameter of the passage was 45 feet and the model rotor was mounted 12 feet above the lowest portion of the duct. These data are presented in figure 15(a).

DISCUSSION

Limitations due to propeller-induced vibrations on the range of variables that could be covered with the aircraft fixed in pitch made it impossible to obtain a direct evaluation of the longitudinal stability and control throughout the autogiro-type and airplane-type flight ranges. The data obtained in the investigation were therefore extended by analytical means in order to determine more completely the characteristics of the convertiplane. In order to evaluate the worth of the analyses,

comparisons of analytical results with applicable full-scale data are included. The details of the analyses are given in Appendix A for horizontal tail characteristics, Appendix B for downwash, and Appendix C for stability and control. A representative gross weight of 5,000 pounds was used throughout since the weight varies in flight from about 4800 to 5300 pounds.

All pitching-moment results apply to the rearmost possible center-of-gravity position. Therefore, the convertiplane stability characteristics reported herein pertain to the least stable extreme.

Due to the differences in rotor behavior, the autogiro-type flight configuration will be considered separately.

Static Angle-of-Attack Stability

Knowledge of the variation of downwash angle and center of pressure with angle of attack is insufficient, in the case of the XV-1, to define the angle-of-attack stability about a given center of gravity location. This is true because the V-tab horizontal tail and the rotor can also be expected to influence angle-of-attack stability characteristics.

The effect of the V-tab horizontal tail on angle-of-attack stability can be determined by examination of the following equation (derived in Appendix A), which defines the tail floating angle.

$$\delta_{ST} = -\frac{\left(\frac{\partial C_{m_T}}{\partial \delta_S}\right)\delta_{S_o} + \left(\frac{\partial C_{m_T}}{\partial \delta_t}\right)\gamma\delta_{T_o} + \frac{6.2}{q\,\frac{q_T}{q}\,S_T c_T}}{\tau\left[\frac{\partial C_{m_T}}{\partial \delta_S} + \gamma\left(\frac{\partial C_{m_T}}{\partial \delta_t}\right)\right] + \frac{0.28}{q\,\frac{q_T}{q}\,S_T c_T}}$$

It can be deduced from this equation that the stick-fixed stability contribution of the V-tab horizontal tail should be the same as if the incidence were constant only insofar as explicit dependence on angle of attack is concerned. However, the velocity at the tail influences (1) the dynamic pressure, q_T, and (2) the trim-tab ratio, γ, and it is apparent that changes in wake-velocity magnitude with angle of attack can combine to change the stabilizer angle, and thus the stability index.

The effect of the rotor lift on the angle-of-attack stability is a result of the vertical displacement of the rotor hub from the center of gravity. This means that the rotor thrust vector need not necessarily act through the center of gravity and thus will introduce moments which can affect angle-of-attack stability.

Autogiro-type flight.- The data of figure 8 show the XV-1 to be unstable with angle of attack at the three test airspeeds. Possible causes are, of course,

1. The adverse variation of downwash angle and wake velocity at the tail with angle of attack.

2. The adverse variation of the magnitude and orientation of the rotor thrust vector with angle of attack.

The effect of downwash and wake-velocity variation on angle-of-attack stability is appraised by means of the equation for the variation of tail angle of attack with fuselage angle of attack as a function of downwash-angle and stabilizer-angle variation with angle of attack. This is

$$\frac{\partial \alpha_T}{\partial \alpha_f} = 1 - \frac{\partial \epsilon_T}{\partial \alpha_f} + \frac{\partial \delta_{ST}}{\partial \alpha_f}$$

Examination of the data shown in figure 15 indicates that $\partial \epsilon_T / \partial \alpha_f$ is nearly unity. Therefore, the first two terms on the right-hand side of the foregoing equation combine in such a way that the angle of attack of the tail is unaffected by changes of downwash angle with angle of attack of the convertiplane. Furthermore the data shown in figure 12 indicate that $\partial \delta_{ST} / \partial \alpha_f$ is negligible. Thus $\partial \alpha_T / \partial \alpha_f$ is approximately zero, which implies that the wake velocity is nearly constant with angle of attack. One can therefore conclude that the tail contribution to angle-of-attack stability is negligible.

An indication of the rotor effect on stability can be deduced from comparison of the $C_{L_T} \cong 0$ pitching-moment curve of figure 6 and the pitching-moment curves of figure 8. From the data in figure 6, it is seen that the contribution of the tail to angle-of-attack stability was zero; in figure 8 the tail moment was constant (contribution to stability was zero). Therefore, the difference in the slope of the pitching-moment curve in figures 6 and 8 is directly attributable to a difference in the magnitude and line of action with respect to the center of gravity of the rotor thrust vector. Thus, adding the rotor to the convertiplane brought about an unstable change in angle-of-attack stability, $\partial C_m / \partial \alpha_f$, of approximately 0.0009 per degree at 100 knots airspeed.

The data in figure 9 show the angle-of-attack stability with reduced rotor lift and the rotor lift allowed to vary with angle of attack. This brings about neutral angle-of-attack stability. Even in this small rotor lift condition, figure 10 shows that the rotor causes an unstable change of $\partial C_m/\partial \alpha_f$ of 0.0005 per degree.

Approximate calculations indicate that the neutral point of the convertiplane was at about 18-percent M.A.C., or 2-percent M.A.C. ahead of the test center of gravity. Therefore, with a forward shift in center-of-gravity location, the convertiplane could be made stable with angle of attack in autogiro-type flight.

The scatter of the data presented in figure 8 is too large to show a change in angle-of-attack stability with speed. However, examination of the downwash data (fig. 15(a)) indicates that, although $\partial \epsilon_T/\partial \alpha_f$ is about unity throughout the autogiro-type flight range, a slight decrease in $\partial \epsilon_T/\partial \alpha_f$ with increasing airspeed occurs at the angles of attack for level flight. This tends to increase stability. In addition, the lift-curve slope of the convertiplane is shown in figure 8 to decrease with increasing airspeed. This change is attributable to the rotor characteristics, and indicates that the variation in rotor thrust with angle of attack decreases with increasing airspeed. These effects probably combine to produce a small increase in angle-of-attack stability with speed.

Angle-of-attack stability for autogiro-type flight could not be determined with the propeller operating because of excessive vibration. However, a comparison of data obtained with the rotor blades removed both with and without powered propeller (fig. 11) shows that the effect of propeller power on stability was negligible. It is believed that the addition of the rotor blades would not significantly alter this result. Therefore, it is believed that the angle-of-attack stability of autogiro-type flight will be unaffected by propeller operation.

In summary, it can be stated that in autogiro-type flight, angle-of-attack stability did not exist for the most rearward center-of-gravity position. This result was a consequence of the variations with angle of attack of rotor downwash, rotor thrust, and line of action of the thrust vector under circumstances where the rotor provided a large portion of the entire lift of the aircraft. Calculations indicate that a 2-percent M.A.C. forward shift of the center of gravity would give neutral angle-of-attack stability. These results assume no lag between convertiplane angle-of-attack changes and rotor rpm changes. The effect of lag will be discussed in the dynamic stability section.

Airplane-type flight.- The convertiplane angle-of-attack stability characteristics in the airplane-type flight configuration are shown by the data in figure 10. These were due primarily to the following rotor characteristics:

1. Rotor lift coefficient constant with angle of attack.

2. Rotor lift small in comparison with the total convertiplane lift.

The implications of these rotor characteristics with respect to angle-of-attack stability factors are:

1. The rotor contribution to downwash at the tail was constant with angle of attack.

2. The change with angle of attack of the rotor lift contribution to pitching moment was small because of the maintenance of small rotor lift.

Item 1 indicates that the V-tab horizontal-tail contribution to stability should be the same with the rotor blades removed as with the convertiplane in the airplane-type flight configuration. Item 2 indicates that the large destabilizing effect of the rotor which is present in the autogiro-type flight configuration would be greatly reduced in the airplane-type flight configuration. Therefore, the angle-of-attack stability with the rotor blades removed should be about the same as the stability of the convertiplane in the airplane-type flight configuration. Comparison of the appropriate curves in figure 10 confirms this. The adverse effect on stability of allowing the rotor lift to vary with angle of attack even though the rotor lift is kept small is shown by the governor-inoperative data replotted from figure 9.

The effect of speed on angle-of-attack stability is shown by the $\delta_{S_o} = 10^\circ$, $\delta_{T_o} = 20^\circ$ curves of figure 10. Comparison of the 100- and 125-knot airspeed curves indicates that little, if any, change in angle-of-attack stability with airspeed occurred for the airplane-type flight configuration. This can be attributed directly to the rotor rpm governor which kept the rotor lift constant.

The effect of powered propeller on angle-of-attack stability with the rotor blades removed is shown by the data of figure 11. Again, the data indicate that very little change in angle-of-attack stability occurred with a constant propeller rpm. These curves are believed indicative of the effect of power on the airplane-type flight configuration as well as on the autogiro-type flight configuration.

It can be concluded that the XV-1 should have angle-of-attack stability in the airplane-type flight configuration. This is primarily a result of keeping the rotor lift coefficient constant with angle of attack.

Static Speed Stability

Speed stability is defined by the slope of the pitching moment versus velocity curve at trim for constant angle of attack and control settings. A positive slope is stable. Speed stability is normally an inherent quality of powered rotors whereas autorotating rotors and airplanes generally have neutral speed stability.

The neutral speed stability associated with the conventional autogiro and airplane can be changed by the introduction of anything which causes an aerodynamic coefficient to depend upon airspeed. Propeller operation, a spring in the control system, and Mach number effects are some of the possible causes of deviation from neutral speed stability by an autogiro or airplane.

The pitching moment of the autorotating rotor in general and the XV-1 rotor in the autogiro-type flight configuration in particular is constant with airspeed because the rotor rpm is free to change with airspeed. This means that for a given blade pitch angle and aircraft angle of attack, the tip-speed ratio, lift coefficient, drag coefficient, and downwash of the rotor tend to remain constant with changing airspeed. The longitudinal data (C_L, C_D) in figure 8 and the downwash-angle data of figure 15(a) show that this is essentially the case for the XV-1 in the autogiro-type flight configuration. In the airplane-type flight configuration, on the other hand, C_L, C_D, μ, and ϵ_T vary with airspeed at a constant angle of attack because the rotor rpm was kept constant. However, the rotor was so lightly loaded ($C_{L_R} \leq 0.03$) that these variables had small effect on the speed stability compared to the effect of the V-tab horizontal tail. From these considerations, it is apparent that rotor-removed data will suffice to determine the speed stability characteristics of the convertiplane.

The important factors affecting speed stability are:

1. Variation of the tail incidence angle with airspeed, including propeller effects, which can be expressed as $\partial\delta_{ST}/\partial V_T$. This brought about:

   (a) A stabilizing tail lift contribution to pitching moment with changing flight airspeed. Examination of figure 14 shows a decrease in tail incidence with increasing airspeed, which produces a nose-up, or stable, pitching-moment variation with airspeed.

   (b) A destabilizing effect from the propeller slipstream. Consideration of the momentum equation for propellers shows that, at a constant engine rpm, the increment of airspeed at the tail would decrease with increasing flight airspeed. This would tend to counteract the effect of item (a).

2. Variation of item 1 with trim-tab setting, which can be expressed as $\partial(\partial\delta_{ST}/\partial V_T)\partial\delta_{T_O}$. Comparison of figures 14(a) and 14(b) shows that the slope of the curve of stabilizer incidence angle versus airspeed increased with increasingly negative trim-tab setting. This indicates an increasing tail contribution to speed stability as the trim-tab deflection becomes more negative.

Because the rotor in both the autogiro-type and airplane-type flight configurations contributes very little to speed stability; the rotor-removed data can be used to determine the speed stability of the XV-1 under both of these conditions. Figure 16 shows the pitching moment versus velocity curves for the rotor-removed configuration. The curves of figure 16 are cross plots of the data in figure 7. The powered-propeller curves in figure 16(c) were calculated by adding a pitching-moment increment due to the powered propeller, obtained from tables II and III, to the rotor- and propeller-removed pitching moments.

Analysis of figure 16 indicates that the pitching moment versus velocity curve for a given angle of attack and velocity is a valid indication of speed stability at each trim-tab setting. The servo-tab setting could be changed to bring about trim, but the speed stability at a given speed did not change. It can therefore be concluded that the XV-1 will have speed stability throughout the flight range investigated with the propeller removed (power off). The magnitude of the power-off stability increases with larger negative trim-tab deflections and decreases with airspeed. The powered propeller decreases speed stability and is very likely to produce speed instability at the higher engine rpm's and smaller trim-tab settings. Large negative trim-tab settings can be expected to improve the powered-propeller instability and may completely eliminate it. The analysis in Appendix A discusses these characteristics more completely.

Longitudinal Stick Motion and Control

A more forward stick position for trim with increasing airspeed is defined as stable stick motion. Possible stick motion instability was evidenced by the XV-1, both with power off (propeller removed) and at rated power, for a trim-tab setting of -20°.

The important factors with respect to stick motion for the given configuration are a combination of the factors discussed in the static angle-of-attack and speed-stability sections. They are:

1. The change in speed stability with α_f (change in angle-of-attack stability with speed), which can be expressed as $\partial(\partial C_m/\partial V)_{C_{m=O}}/\partial\alpha_f$ or $\partial(\partial C_m/\partial\alpha_f)_{C_{m=O}}/\partial V$.

2. Variation of downwash at the tail with α_f, which can be expressed as $\partial\epsilon_T/\partial\alpha_f$.

3. Control linkage characteristics, which can be expressed as $\partial V_{C_m=o}/\partial\delta_{S_o}$.

4. Horizontal-tail characteristics with airspeed, which can be expressed as $\partial\delta_{ST}/\partial V_T$ and $\partial(\partial\delta_{ST}/\partial V_T)/\partial\delta_{T_o}$. Of these variables, the trim-tab setting was the most easily changed. Therefore, an analysis was conducted to determine the stick motion characteristics at a trim-tab setting of -60°. The details of the analysis are given in Appendix C.

Figures 17(a) and (b) present data showing the variation of pitching moment to be trimmed out as a function of airspeed for certain test conditions. The pitching moments to be trimmed out were obtained from figure 8 or 10, depending on the convertiplane configuration in question. These data were chosen at the lift coefficient required for level flight at each airspeed. The powered-propeller data at a trim-tab setting of -20° were obtained by adding an increment in pitching moment due to the powered propeller from table III to the power-off pitching moment obtained from figure 8 or 10. The powered-propeller data at a trim-tab setting of -60° were calculated by the method described in Appendix C. The changes in servo-tab deflection required to balance the moments discussed above were obtained from the calculated V-tab horizontal-tail characteristics shown in figure 18 and the corresponding curves of the stick position required for trim versus airspeed. These data are shown in figures 17(c) and (d). These calculations are believed to give only the gross effects of power and control setting.

Autogiro-type flight.- Analysis of figure 17(c) indicates:

1. Power-off stick motion with changing airspeed at $\delta_{T_o} = -20°$ is unstable for the low-speed end and neutrally stable at the high-speed end of the autogiro-type flight range.

2. The effect of powered propeller on stick motion with changing airspeed is to produce instability at $\delta_{T_o} = -20°$. The stick travel required for trim exceeds the forward limit at airspeeds less than about 80 knots, so that the convertiplane then becomes uncontrollable.

3. The effect of changing the trim-tab deflection to -60° under the conditions in item 2 would bring about stable stick motion with changing airspeed. This change in trim-tab setting places the stick position for trim well within the control limits.

It can be concluded that the XV-1 in the autogiro-type flight configuration can have stick motion stability with powered propeller at a trim-tab setting of -60°. Moreover, it is believed that the XV-1 can have stick motion stability and be controllable at a trim-tab setting as low as -40°. Free-to-float tests qualitatively support this conclusion.

Airplane-type flight.- Because of the difference in rotor characteristics, there is considerable change in the stick position variation with airspeed between the autogiro- and airplane-type flight configurations. Analysis of figure 17(d) indicates:

1. Stick motion with power off is stable at $\delta_{T_O} = -20°$ in the airplane-type flight range investigated.

2. The effect of powered propeller on stick motion is to produce almost neutral speed stability at $\delta_{T_O} = -20°$. The stick position for trim is well within the control limits.

3. The effect of changing the trim-tab deflection to -60° under the conditions in item 2 would bring about stable stick motion. This trim-tab setting places the stick position for trim well within the control limits.

It can be concluded that the XV-1 in the airplane-type flight configuration can have stick position stability with powered propeller at large negative trim-tab settings. It is believed that the XV-1 in the airplane-type flight configuration can have stable stick motion and be controllable at the same trim-tab settings ($\delta_{T_O} = -40°$ to -60°) appropriate to autogiro-type flight. Free-to-float tests qualitatively support this conclusion.

An interesting property of the V-tab horizontal tail is its ease of modification. Increased stiffness of the trim-tab spring would provide greater control effectiveness, if needed, without large aircraft modifications. An increase in the stiffness of the spring would, however, reduce the speed stability contribution of the horizontal tail as indicated by the analysis in Appendix A.

Longitudinal Dynamic Stability

Within limits, indications of the dynamic stability characteristics of the convertiplane could be obtained from the free-to-pitch test results. The results are only an indication because of the constant tunnel airspeed, friction damping in the support system, and restraint in vertical translation.

In the autogiro-type flight configuration the small amount of pitch freedom (1/2°) did not allow determination of the stability characteristics. However, it is probable that the convertiplane would not be as susceptible to instability during gusts and pull-up maneuvers as the static angle-of-attack stability discussion would indicate. This is possible because of the lag between changes in convertiplane angle of attack and corresponding changes in rotor rpm. In conditions such as these, the convertiplane would probably be as stable in the autogiro-type configuration as in the airplane-type configuration.

In the airplane-type flight configuration, the tests indicated the aircraft would be dynamically stable with angle of attack. Dynamic instability did occur in the airplane-type flight configuration when the rotor rpm governor had too much lag. Several slight modifications to the governor corrected the excessive lag and made the convertiplane dynamically stable.

Interference Between the Fixed Wing and Rotor

Because of the general interest in the effect on an aircraft of combining a rotary wing and a fixed wing, the data in figures 19 and 20 were replotted from figures 7, 8, and 10 in order to compare directly the lift and drag contributions of the aircraft components in both the autogiro-type and airplane-type flight configurations. Included are full-scale rotor-alone data obtained from reference 2.

Autogiro-type flight.- The data in figure 19 indicate that the measured lift in the autogiro-type flight configuration was less than the sum of the rotor-removed and the rotor-alone lift for corresponding values of wing angle of attack and rotor tip-speed ratio. This result is not surprising for a biplane lifting system. Since the most tangible factor causing the difference is the reduction in actual wing angle of attack caused by the rotor downwash, the calculated reduction in wing angle of attack (based on the theory of ref. 5) from this source is shown in figure 21. For comparison, the change in wing angle of attack which would be needed to account for the entire lift difference in question is also plotted. The comparison indicates that rotor downwash can account for most of the difference under some conditions and about half of it for the remaining conditions.

The effect on the lift-drag ratios brought about by adding the lifting rotor to this aircraft is shown below. The data presented are at the angle of attack of the complete convertiplane required for level flight at three airspeeds. The isolated rotor data in the two columns below were chosen to match the corresponding rotor-tip-speed ratio and nominal rotor-blade pitch setting of the complete aircraft.

V, knots	α_f, deg	μ	L/D						
			Complete aircraft	Sum of components	Rotor blades removed	Rotor blades alone	Rotor blades and hub[1]	Theory (clean blade) ref. 6	Theory (including hub drag)
75	3.65	0.23	4.8	5.4	7.7	4.8	4.5	6.8	6.3
100	.65	.32	5.0	5.8	6.2	5.6	4.9	9.1	7.4
125	-1.4	.41	4.1	5.2	4.6	5.7	4.6	10.9	7.4

[1]The addition of the hub caused air-flow separation on the pylon. These data include both the hub profile drag and the air-flow separation drag.

The lift-drag ratios of the complete aircraft were appreciably less than those derived on the basis of the sum of the components. This may be attributed to the interference inherent in a biplane lifting system.

Theoretical rotor lift-drag ratios calculated from reference 6 are included above. Considerable discrepancy between the experimental rotor data and theoretical predictions is evident. Two possible explanations for the lower experimental values are (1) rotor blade profile drag higher than estimated in reference 6, and (2) rotor hub and pylon air-flow-separation drag neglected in the theoretical calculations. It is believed that the discrepancy at 75 knots was due principally to item 1. This was caused by tip burners, strain gages, and so on. It can be noted that the theoretically predicted trend toward higher lift-drag ratios with increasing tip-speed ratio was not shown by the test data. It is believed that this was partially due to the increasing importance of the hub- and air-flow-separation drag with forward speed of the aircraft. In an attempt to account for this type of rotor drag, the measured hub and air-flow-separation drag ($\Delta C_D = 0.0039$) was used to modify the theoretical lift-drag ratios. The result of this calculation is compared above with the rotor-blades and hub data. This comparison indicates that the theory of reference 6, when concerned with practical rotors, may be seriously limited at the higher airspeeds because of the difficulty in accurately estimating the drag of rotor components such as the hub, exposed linkages, and mounting structure.

Airplane-type flight.- Figure 20 shows that in the airplane-type flight configuration, interference between the fixed wing and rotor still exists, the complete aircraft lift being less than the sum of the component lifts.

A summary of the effect of the rotor in the airplane-type configuration on the airplane lift-drag ratios is listed below for the angle of attack of the convertiplane required for level flight at 125 knots.

Configuration	L/D
(a) Aircraft with rotor blades removed (includes hub-and air-flow-separation drag)	7.2
(b) Rotor-blades alone	4.0
(c) Convertiplane	5.6
(d) Sum of the aircraft components ((a) + (b))	5.8

It can be seen from the foregoing data that the addition of even a lightly loaded rotor to an airplane will reduce the airplane efficiency significantly. In comparison, it can be pointed out that the lift-drag ratios of conventional airplanes having the same gross weight and maximum speed are in the neighborhood of 10.

Aircraft Drag

A study was made to determine the drag contributions of the various aircraft components in order to find out if the sea-level performance could be improved.

The drag tests consisted of two parts: (1) Attempts to reduce the air-flow separation due to hub-pylon interference, and (2) a general aircraft clean-up.

Hub-pylon interference.- Flow separation on the pylon due to the influence of the rotor hub had been noted in small-model tests, and tuft studies on the full-scale aircraft confirmed the small-model tests in this respect. The tuft studies showed that the separated area extended from the top of the pylon at the rotor center line down diagonally across the pylon as shown at the top of figure 5. Even with unseparated flow, obtained with the high fairing and sealed joints, the tufts indicated a downward flow on the pylon. It is believed that the flow separation originated at about the maximum-thickness point on the rotor-shaft housing, between the hub and the pylon. Modifications made to the pylon in an attempt to stop the air-flow separation are shown in figure 5. A list of the drag increments realized by some of the modifications is presented below. In all the high fairing configurations, the rotor blades were removed.

Configuration	ΔC_D
High fairing	0.0002
High fairing, all joints sealed	-.0022
High fairing, low fence	.0003
High fairing, high fence	.0003

A significant drag decrease was brought about by use of a high fairing only with all the joints sealed. That the reduction in drag resulted from elimination of the air-flow separation on the pylon was shown by tuft studies; the high fairing would not, however, allow the rotor to rotate. Thus, it is not known if the rotating rotor would have caused separation with the high fairing. In all cases, fences increased the drag.

An attempt was made to control the air-flow separation on the pylon by removing the separated air through perforated areas and holes. The autorotating rotor was used as a pump. No decrease in drag was evidenced by the available suction through the perforated areas. Suction through the holes decreased the drag coefficient by 0.0003, but the tufts indicated the same separated region. Fences used with the holes brought about a net increase in drag. Although suction-air quantity was not measured, it is probable that insufficient air was drawn through the perforated areas and suction holes. In addition, the perforated areas and suction holes may not have been in advantageous locations.

Aircraft clean-up.- Aircraft clean-up was the other attempt at drag reduction. In the clean-up programs, external protuberances were faired and gaps were sealed. Various components of the aircraft were removed and their drag contribution determined. Finally, the drag contribution of the support system was evaluated. The results of the clean-up are listed below for the angle of attack corresponding to level flight in the airplane-type configuration at 125 knots. Drag coefficient of the aircraft before the clean-up was 0.0230 at the angle of attack required for level flight at 125 knots.

Configuration and components	ΔC_D
Rotor blades and hub sealed and faired	0.0000
Normal pylon, gaps sealed	.0000
All practicable fairings	-.0004
Rotor blades removed	-.0063
Hub removed	-.0039
Tail-fan assembly, pitot static mast, wing-tip skids removed	-.0002
Engine ducting unsealed	.0006
Skid landing gear removed	-.0019
Pitch strut and pitch-strut fairings removed	.0000
Lift struts	-.0006

Of the component drags listed above, the rotor blades and hub account for 0.0102 or 45 percent of the total. If the hub-pylon interference drag were eliminated, the rotor blades and hub drag would account for 0.0080 out of 0.0208, or 38 percent of the total. This is in the configuration where the rotor is merely an appendage to the convertiplane. Therefore, in comparisons of the XV-1 type convertiplane with conventional aircraft,

the inherent high drag of the autorotating rotor system, even with low rotor lift, introduces a severe performance penalty during high-speed operation.

When the landing skids, tail-fan assembly, pitot static mast, and wing-tip skids were removed, and all practicable fairings were used, the reduction in drag coefficient was 0.0025. In addition, when the pylon air-flow separation was completely eliminated the total drag reduction was 0.0047 or about one-fifth of the drag existing with the airplane-type configuration at 125 knots.

Figure 22 shows the improvement in performance due to the aircraft clean-up program in the horsepower versus airspeed form. The reduction in drag that would be realized if the air-flow separation on the pylon were completely eliminated is not included. An increase in maximum speed of the aircraft from 120 to about 130 knots at rated power is indicated if the drag coefficient is reduced by 0.0025.

CONCLUSIONS

Results of the full-scale wind-tunnel investigation indicate that the XV-1 convertiplane should successfully accomplish the autogiro-type and airplane-type portions of its prescribed flight plan. Unexpectedly high drag, however, could seriously limit performance.

In regard to longitudinal stability, control, and performance characteristics:

1. By proper choice of trim-tab setting the convertiplane can be made statically stable with respect to speed and stick motion with the center of gravity at the most rearward position throughout the airspeed range investigated. Longitudinal control should be adequate, provided that large negative trim-tab settings are used.

2. The convertiplane was statically unstable with angle of attack in the autogiro-type flight configuration. This was with the center of gravity at the most rearward position.

3. The loss in lift due to interference between the fixed wing and the rotor could not be calculated accurately using simple premises. This interference caused the lift-drag ratios of the complete aircraft to be appreciably less than those calculated from the individual component data.

4. Although the rotor contributes little lift during airplane-type flight, the rotor blades, rotor hub, and hub-pylon interference are responsible for 45 percent of the total drag. If the hub-pylon interference drag were eliminated, the rotor and its hub would contribute about 38 percent (based on the revised total drag) of the total convertiplane drag.

5. Use of the methods developed in the appendices, along with the downwash theory of NACA TN 2912, permits a reasonably accurate estimate of the tail-contribution to longitudinal stability and control parameters.

Ames Aeronautical Laboratory
National Advisory Committee for Aeronautics
Moffett Field, Calif., Nov. 21, 1955

APPENDIX A

ANALYSIS OF A V-TAB HORIZONTAL TAIL

Consideration of the longitudinal stability and control problems of a convertiplane indicates that a free-floating horizontal tail can be made to give desirable contributions to the aircraft's longitudinal characteristics.

A survey of free-floating tail configurations indicates that a satisfactory design from the standpoint of small control forces, rapid response, and freedom from dynamic instability is one where the hinge line is located at the aerodynamic center. Although hinging a surface behind the aerodynamic center contributes more to longitudinal stability, the analysis herein deals only with the former arrangement to avoid the complications due to the dynamic problems associated with the latter.

Modifications necessary to the horizontal tail hinged at the aerodynamic center are (1) a servo tab for control and (2) a linkage between the stabilizer and the tabs to provide artificial stability of the tail with respect to itself. It would be convenient, for the sake of control, to have a trim tab on the tail so that control position could be varied. If the linkage were also connected to the trim tab, more positive stabilization of the tail would result; consequently, it will be assumed that the linkage would be used on both tabs. Properties of the free-floating tail mounted at the aerodynamic center with the aforementioned controls and linkages are (1) the stabilizer incidence constant with angle of attack, (2) stabilizer incidence dependent only on the relationship between the servo and trim tabs. Since the stabilizer-tab linkage makes the tab angles dependent on stabilizer angle, the stabilizer must adjust its incidence until an equilibrium position is reached. These tail characteristics make the tail similar to an all-movable horizontal tail. For this configuration the linkage between the servo tab and stick can be adjusted to give the proper stick motion. The tail, as described thus far, can provide stick-motion stability.

Speed stability properties can be introduced into the horizontal-tail system by spring loading the trim tab so that the actual trim-tab deflection is a function of airspeed as well as the stabilizer angle and tab setting. The result of the spring-loaded trim tab in the system is that the stabilizer angle becomes increasingly negative with increasing airspeed, the magnitude depending on the trim-tab spring rate.

In the usual configuration, the trim-tab spring may not be required since neutral speed stability is generally acceptable; however, in the case of the XV-1, the location of the horizontal tail in the propeller

slipstream might introduce a large destabilizing effect on speed stability. Therefore, the trim-tab spring acted in a direction to improve speed stability.

On the XV-1, an additional spring was incorporated to hold the stabilizer at an incidence angle of 60° to 40 knots flight speed in order to avoid large down loads from the rotor downwash in helicopter flight. At speeds greater than 40 knots the tabs became effective and the tail had sufficient aerodynamic moment to overcome the stabilizer downspring.

In order to understand better the flying tail properties, the governing factors are presented in equation form. A similar analysis is presented in reference 1. The stabilizer-tab linkage ratio is defined as

$$\tau = \left(\frac{\partial \delta_T}{\partial \delta_{ST}}\right)_{\delta_{T_o}} \quad \text{or} \quad \left(\frac{\partial \delta_S}{\partial \delta_{ST}}\right)_{\delta_{S_o}} \tag{A1}$$

Then actual tab deflection is, for the linear range,

$$\delta_S = \delta_{S_o} + \left(\frac{\partial \delta_S}{\partial \delta_{ST}}\right)\delta_{ST} = \delta_{S_o} + \tau\delta_{ST} \tag{A2}$$

$$\delta_T = \delta_{T_o} + \left(\frac{\partial \delta_T}{\partial \delta_{ST}}\right)\delta_{ST} = \delta_{T_o} + \tau\delta_{ST} \tag{A3}$$

The effect of spring loading the trim tab can be expressed as

$$\delta_t = \gamma\delta_T$$

for a given configuration in incompressible flow

$$\gamma = \frac{\delta_t}{\delta_T} = f(V) \tag{A4}$$

The hinge moment introduced by the trim-tab spring can be expressed as

$$C_{h_{spring}} = \frac{K(\delta_T - \delta_t)}{q \frac{q_T}{q} S_t c_t}$$

Furthermore, at some equilibrium position, the hinge moment of the trim tab must equal the moment of the trim-tab spring

$$C_{h_\alpha}(\alpha_T) + C_{h_\delta}(\delta_t) = \frac{K(\delta_T - \delta_t)}{q \frac{q_T}{q} S_t c_t} \tag{A5}$$

substituting equations (A3) and (A4) into equations (A5) yields

$$\gamma = \frac{K\left(\delta_{T_o} + \tau\delta_{ST}\right) - C_{h_\alpha}(\alpha_T) q \frac{q_T}{q} S_T c_T}{\left(C_{h_\delta} q \frac{q_T}{q} S_t c_t + K\right)\left(\delta_{T_o} + \tau\delta_{ST}\right)} \tag{A6}$$

In comparison with C_{h_δ}, C_{h_α} is small. This is verified by comparison of the computed curves in figure 13 in which the simpler equation for γ

$$\gamma = \frac{K}{C_{h_\delta} q \frac{q_T}{q} S_T c_T + K} \tag{A7}$$

is compared with equation (A6). The value of -0.0064 for C_{h_δ} used for the computations was obtained from reference 7.

An equation for the stabilizer angle may be obtained by writing the equation for the moments about the stabilizer hinge line.

$$C_{m_T} = \text{balance moment} + \delta_S\left(\frac{\partial C_{m_T}}{\partial \delta_S}\right) + \delta_t\left(\frac{\partial C_{m_T}}{\partial \delta_t}\right) + \text{downspring moment} = 0 \tag{A8}$$

Calculations showed that the moment due to tail and tab unbalance was negligible for the XV-1. In the linear range the downspring moment equals $6.2 + 0.28\delta_{ST}$ foot-pound per degree (fig. 4(b)). The substitution of equations (A2), (A3), and (A4) into equation (A8) leads to the following expression for δ_{ST}:

$$\delta_{ST} = -\frac{\left(\frac{\partial C_{m_T}}{\partial \delta_S}\right)\delta_{S_o} + \left(\frac{\partial C_{m_T}}{\partial \delta_t}\right)\gamma\delta_{T_o} + \frac{6.2}{q\,\frac{q_T}{q}\,S_T c_T}}{\tau\left[\left(\frac{\partial C_{m_T}}{\partial \delta_S}\right) + \gamma\left(\frac{\partial C_{m_T}}{\partial \delta_t}\right)\right] + \frac{0.28}{q\,\frac{q_T}{q}\,S_T c_T}} \tag{A9}$$

Equation (A9) is evaluated by the comparison of the theoretical, experimental full-scale, and interpolated small-model data showing the change in stabilizer angle with airspeed for several trim and servo-tab combinations in figure 14. The value of -0.0044 for $(\partial C_{m_T}/\partial \delta_S)$ or $(\partial C_{m_T}/\partial \delta_t)$ was obtained from reference 8. As can be seen, equation (A9) provides a fair estimate of the absolute values of stabilizer angle and a good estimate of the slope of the curve of stabilizer angle versus airspeed. The lack of correlation was traced to the difficulty in accurately determining the trim-tab ratio, γ. Substitution of experimental values of γ in equation (A9) gave calculated agreement within $1/2^{\circ}$.

In view of this, it is concluded that the simplified analysis presented herein can be expected to provide reliable estimates of the V-tab free-floating horizontal-tail contribution to longitudinal stability and control parameters.

The change in pitching moment of the complete aircraft with servo-tab or trim-tab setting may then be calculated by the usual equation for the horizontal-tail contribution to pitching moment.

$$\Delta C_m = \frac{l_T}{R}\frac{S_T}{S_R}\frac{q_T}{q}a_T\Delta\delta_{ST} \tag{A10}$$

This equation was used to calculate the V-tab floating-tail effectiveness shown in figure 18.

APPENDIX B

ESTIMATION OF ROTOR DOWNWASH

In order to estimate the stability characteristics of an aircraft, it is essential to know the downwash-field properties with some accuracy. Therefore, an evaluation of the existing downwash theory as applied to the XV-1 type of aircraft was considered to be of interest.

Figure 15(a) compares the downwash angles calculated using the theories of references 5 and 9 with the downwash measured from the V-tab floating tail in the investigation reported herein. Reference 9 allows calculation of downwash through the rotor disk only. Reference 5 extends the theory of reference 9 to allow calculation of the downwash angle at any point in the flow field.

In order to calculate the resultant velocity at any point in the rotor wake and thus the angle between the axis of the wake and the free-stream direction, the following must be known: C_T, μ, and angle of the tip path plane with respect to the free-stream direction. When these are known, the vertical component of the velocity at a desired point in the flow field can be calculated or read from the charts provided. Then the downwash angle can be calculated from

$$\epsilon = \tan^{-1} \frac{w}{V}$$

For the XV-1, full-scale rotor data from previously conducted tests were available so that the rotor-alone lift could be accurately obtained for a set of given conditions. With these experimental values, the vertical component of the velocity, w, at the tail could be calculated and the downwash angle at the tail due to the rotor determined.

For the XV-1, both the rotor and the wing contribute to downwash at the tail. In order to allow for the unloading of the wing by the rotor, the average change in angle of attack of the wing due to the rotor downwash was calculated as outlined above for the case of the tail. These calculations are shown in figure 21. The corresponding downwash due to the wing for the revised angle of attack of the wing ($\alpha_f - \epsilon_w$) was found from figure 15(b) and added to the calculated rotor-alone downwash to give the curves presented in figure 15(a).

As can be seen in figure 15(a), the full-scale and small-model measured downwash at the tail were in good agreement, but the calculated absolute values show poor agreement with experimental absolute values and only fair agreement with respect to slope. However, stabilitywise, slope is the most important. In view of this, it can be concluded that the theory presented in references 5 and 9 will provide estimations of the downwash at the tail with sufficient accuracy to permit first-order approximations of the longitudinal stability parameters of an XV-1 type aircraft.

APPENDIX C

ESTIMATION OF STICK-MOTION STABILITY

In order to obtain an indication of the effect of trim-tab setting on stick-motion stability for both aircraft configurations considered herein, it was necessary to extend the limited data obtained in the wind tunnel. This was necessary since very little data were obtained in this investigation with large negative trim-tab settings and the propeller and rotor operating simultaneously.

As mentioned in the discussion of stick-motion stability, the curve of pitching moment at the lift coefficient required for level flight at a given airspeed versus airspeed for constant control settings can be used to calculate the stick position for trim variation with flight airspeed. The procedure followed and assumptions employed in calculating a curve of this type are presented below.

The analysis in Appendix A provides a means of determining the stability contribution of the horizontal tail for a range of trim- and servo-tab deflections over a range of velocities. The calculated characteristics are shown in figures 14 and 18. The degree of reliability that can be expected from the analysis in Appendix A is shown by the comparisons made in figures 13 and 14 with experimental values. Since the tail characteristics are a function of airspeed at the tail, the additional increment of velocity at the tail due to the propeller slipstream must be considered before applying the results of the analysis in Appendix A to estimate stick-position stability at another trim-tab setting.

Evaluation of Method

In order to establish a valid method of calculating the increase in airspeed at the tail due to the powered propeller and its effect on the pitching moment, calculations were made for conditions which corresponded to available data points. The method of the calculation was as follows:

1. The velocity increment at the tail due to the propeller slipstream was calculated by the momentum method, assuming 25-percent propeller disk blockage.

2. A ΔC_m due to the change in airspeed at the tail was found from figures 18(a) and (b).

3. The ΔC_m of item 2 was corrected to free-stream q.

4. The ΔC_m due to the propeller thrust acting on a point away from the moment center was calculated.

5. The ΔC_m's of items 3 and 4 were added to the propeller-removed data to give the final estimation.

A comparison between the measured data and calculated data is presented below.

V, knots	75			100			125
Propeller rpm	1500	2100	2250	1500	2200	2350	2400
C_m, experimental	0.016	0.025	0.029	0.013	0.022	0.024	0.010
C_m, computed	0.025	0.031	0.037	0.012	0.019	0.022	0.007

The data at 75 and 100 knots are for a constant angle of attack for each airspeed with a trim-tab setting of -20° and a servo-tab setting of 10°. The aircraft was in the autogiro-type flight configuration. The data at 125 knots are for the same tab settings, but with the rotor blades removed.

Although the agreement between computed and experimental values of pitching moment was acceptable at 100 knots, the agreement was poor at 75 and 125 knots. This lack of agreement is believed to be mainly due to the inadequacy of the momentum theory used to predict the average change in velocity at the horizontal tail. Based on the foregoing comparison, correction factors to the calculated velocity at the tail were obtained for each free-stream velocity and power setting shown above. The correction factors were extrapolated to the desired engine rpm.

Estimation of Pitching-Moment Increment Due to Trim-Tab Deflection

The effect of changing the trim-tab deflection from -20° to -60° with powered propeller was calculated by the following method:

1. Velocity at the tail was calculated by the momentum theory and corrected by the required factor.

2. The ΔC_m caused by a change in trim-tab setting from -20° to -60° at the appropriate tail airspeed was found from figure 18.

3. The ΔC_m of item 2 was corrected to free-stream airspeed.

4. The ΔC_m of item 3 was added to the powered-propeller pitching moment for $\delta_{S_o} = 10^\circ$, $\delta_{T_o} = -20^\circ$ (shown in figs. 17(a) and (b)) to give the $\delta_{S_o} = 10^\circ$, $\delta_{T_o} = -60^\circ$ pitching moments.

Estimation of Stick Position for Trim

The stick position for trim was calculated using the above pitching-moment increments. A point by point construction of the curves is shown in figures 17(c) and (d). The method was as follows:

1. The pitching moments for $\delta_{S_o} = 10^\circ$, $\delta_{T_o} = -60^\circ$ of item 4 above were changed in order to reference them to the actual tail airspeed. The ΔC_m to be trimmed out by the servo tab was then obtained from figure 18.

2. The servo-tab setting for trim was then found from figure 18(b). This was converted to equivalent stick position by use of the equation

$$\beta = 1.9\,\delta_{S_o} - 21.6$$

Accuracy of Calculated Tail Characteristics

Because of the influence the calculations shown in figure 18 can have on the stick-motion stability analysis, an indication of the accuracy that can be expected from figure 18 is given below. The data show the experimental $\Delta C_m/\Delta V$ from figure 16(b) and the corresponding calculated values.

Trim-tab setting	$\Delta C_m/\Delta V$, experimental	$\Delta C_m/\Delta V$, calculated
-20°	0.00017	0.00014
-40°	.00023	.00022

These comparisons indicate that the accuracy of equations (A9) and (A10) and the curves in figure 18 were sufficient for use in estimating the stick-motion stability shown in figure 17.

REFERENCES

1. Hohenemser, K. H.: The Development of a V-Tab Controlled Floating Horizontal Tail for Rotary-Fixed Wing Aircraft. McDonnell Aircraft Corp. Report No. 3371, Jan., 1954.

2. Hohenemser, K. H.: Full Scale Rotor Tests of the Air Force Convertiplane Model XV-1 in the NACA 40- by 80-Foot Wind Tunnel at Moffett Field, Calif. McDonnell Aircraft Corp. Report No. 3379, Feb. 1954.

3. Hohenemser, K. H.: The Characteristics of the Model XV-1 Convertiplane in Airplane and in Autogiro Phase Flight Conditions as Measured in the NACA 40- by 80-Foot Wind Tunnel at Moffett Field, Calif. McDonnell Aircraft Corp. Report No. 3599, Nov., 1954.

4. Hohenemser, Kurt: A Type of Lifting Rotor With Inherent Stability. Jour. Aero. Sci., vol. 17, no. 9, Sept. 1950, pp. 555-564.

5. Castles, Walter, Jr., and DeLeeuw, Jacob Henri: The Normal Component of the Induced Velocity in the Vicinity of a Lifting Rotor and Some Examples of Its Application. NACA TN 2912, 1953.

6. Bailey, F. J., Jr., and Gustafson, F. B.: Charts for Estimation of the Characteristics of a Helicopter Rotor in Forward Flight. I - Profile Drag-Lift Ratio for Untwisted Rectangular Blades. NACA WR L-110, 1944.

7. Sears, Richard I.: Wind-Tunnel Data on the Aerodynamic Characteristics of Airplane Control Surfaces. NACA WR L-663, 1943.

8. Ames, Milton B., Jr., and Sears, Richard I.: Determination of Control Surface Characteristics from NACA Plain-Flap and Tab Data. NACA Rep. 721, 1941. (Formerly NACA TN 796)

9. Coleman, Robert P., Feingold, Arnold M., and Stempin, Carl W.: Evaluation of the Induced Velocity Field of an Idealized Helicopter Rotor. NACA WR L-126, 1945.

TABLE I.- PHYSICAL CHARACTERISTICS OF THE XV-1 CONVERTIPLANE

Rotor	
Diameter, ft	31
Disk area, sq ft	758
Solidity ratio (or factor)	0.09
Airfoil	NACA 63_2A(1.5)15
Blade twist, center to tip, deg	-8
Blade chord, ft	1.162
Mass constant, per radian	4.2
Wing	
Area, sq ft	99.6
Aspect ratio	6.76
Span, ft	26
M.A.C., ft	3.91
Airfoil	NACA 63_2A215
Incidence of inner panel, deg	8
Incidence of outer panel at boom, deg	8
Incidence of outer panel at tip, deg	5
Dihedral, deg	0
Sweepback of the quarter-chord line, inner panel, deg	0
Sweepback of the quarter-chord line, outer panel, deg	11.5
Horizontal tail	
Area, sq ft	16.97
Span, ft	8.17
Chord, ft	2.08
Aspect ratio	3.92
Hinge-line location, percent chord	22.5
Airfoil	NACA 0012
Distance from rotor center line to tail hinge line, ft	16.71
Tabs	
Area, sq ft	1.28
Span, ft	4.08
Chord, ft	0.312
Spring constant (trim tab only), per deg	-0.05 ft-lb
Overhang	0.10 c_t
Gap	0.01 c_t

TABLE II.- AERODYNAMIC DATA WITH POWERED PROPELLER AND ROTOR BLADES REMOVED; V = 125 KNOTS

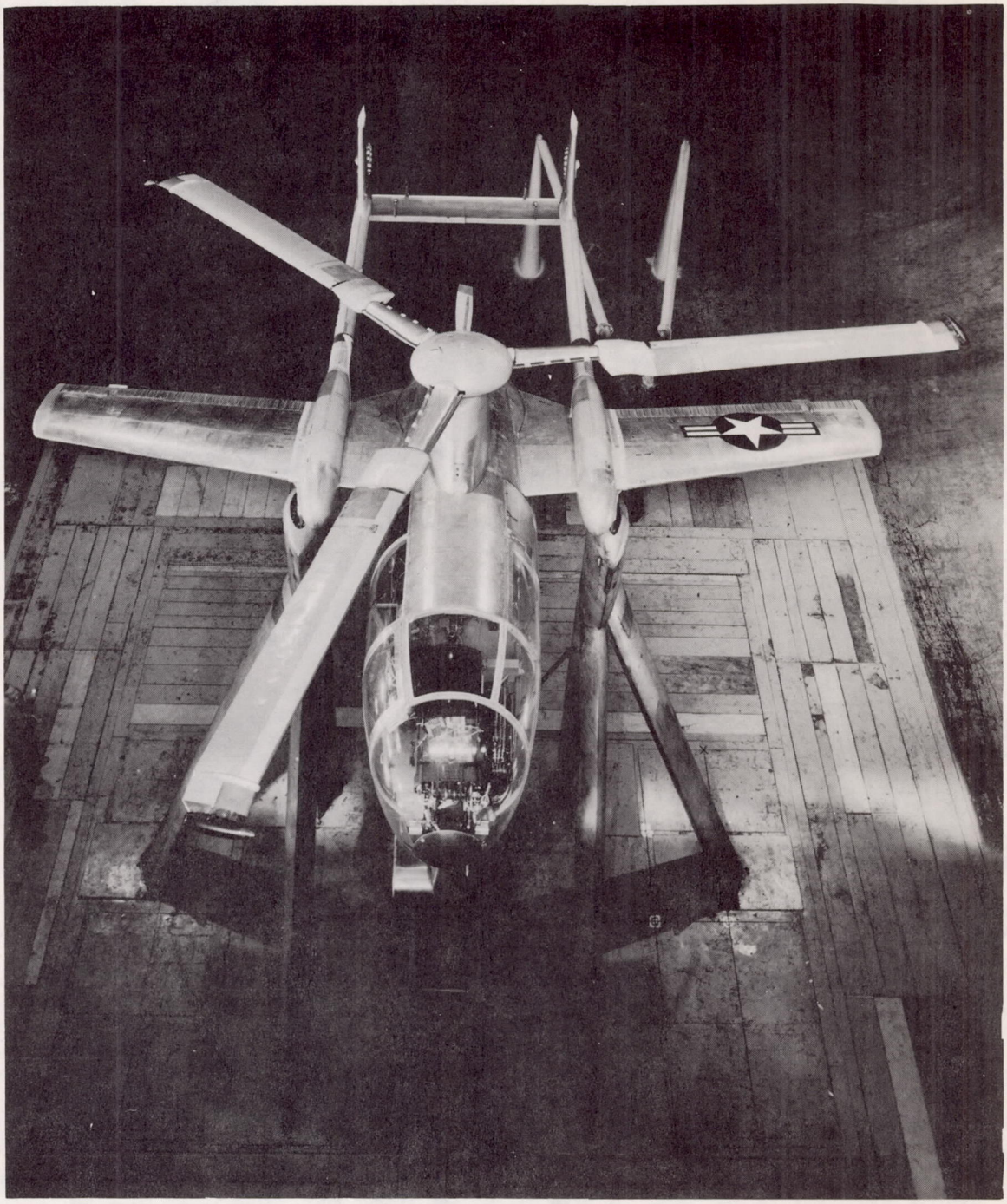
δ_{S_o}, deg	δ_{T_o}, deg	α_f, deg	Engine rpm	C_L	C_D	C_m
10	-20	-2	2400	0.044	-0.0063	0.0110
10	-20	0	2400	.070	-.0060	.0100
10	-20	2	2400	.095	-.0051	.0083
10	-20	4	2400	.119	-.0034	.0068
10	-20	6	2400	.142	-.0014	.0048
5	-20	-2	1500	.053	.0107	-.0005
5	-20	0	1500	.078	.0116	-.0029
5	-20	2	1500	.101	.0127	-.0045
5	-20	4	1500	.123	.0145	-.0060
5	-20	6	1500	.144	.0168	-.0074
5	-20	-2	2400	.050	-.0072	.0046
5	-20	0	2400	.074	-.0067	.0036
5	-20	2	2400	.098	-.0056	.0019
5	-40	-2	2400	.053	-.0063	-.0069
5	-40	0	2400	.078	-.0057	-.0079
5	-40	-2	1500	.057	.0121	-.0115
5	-40	0	1500	.080	.0128	-.0120
11.5	-30	-2	1500	.07	.0114	(1)
12	-30	0	1500	.07	.0117	↓
13	-30	2	1500	.10	.0126	↓
14	-30	4	1500	.12	.0145	↓
15	-30	6	1500	.14	.0171	↓
5	-30	-2	2400	.06	-.0072	↓
6	-30	0	2400	.07	-.0071	↓
8	-30	2	2400	.10	-.0050	↓
9	-30	4	2400	.12	-.0035	↓
10	-30	6	2400	.15	-.0007	↓

[1]Aircraft free to float

TABLE III.- AERODYNAMIC DATA WITH POWERED PROPELLER

V, knots	δ_{S_o}, deg	δ_{T_o}, deg	α_f, deg	Configuration[1]	Rotor rpm	Engine rpm	C_L	C_D	C_m	V, knots	δ_S, deg	δ_T, deg	α_f, deg	Configuration	Rotor rpm	Engine rpm	C_L	C_D	C_m
75	10	-20	0	2	178	2250	0.093	-0.0360	0.0190	100	0	-30	-1	2	180	1500	0.09	0.0149	(2)
75	10	-20	2	2	178	2250	.119	-.0352	.0187	100	5	-30	-1	2	180	1500	.08	.0177	
75	10	-20	4	2	178	2250	.147	-.0335	.0163	100	0	-30	-1	2	175	1500	.09	.0145	
75	10	-20	6	2	178	2250	.171	-.0309	.0126	100	0	-30	-1	2	175	1800	.09	.0073	
75	10	-20	4.2	1	345	1500	.372	.0598	.0165	100	0	-30	-1	2	175	2250	.09	-.0074	
75	10	-20	4.2	1	345	2100	.361	.0286	.0249	100	10	-30	2	1	330	1500	.22	.0400	
75	10	-20	4.2	1	345	2250	.356	.0185	.0290	100	11	-30	3	2	175	1500	.14	.0174	
75	5	-30	3	1	325	1500	.332	.0514	-.0008	100	1.8	-30	0	1	325	1500	.20	.0337	
75	5	-40	3	1	325	2300	.333	.0110	-.0040	100	5	-40	0	1	325	2300	.19	.0058	
100	10	-20	0	2	175	2350	.084	-.0153	.0159	125	0	-30	-1	2	175	1500	.08	.0177	
100	10	-20	2	2	175	2350	.109	-.0137	.0129	125	5	-30	2	2	175	1500	.12	.0201	
100	10	-20	4	2	175	2350	.135	-.0127	.0117	125	5	-30	2	2	175	1900	.12	.0147	
100	10	-20	6	2	175	2350	.157	-.0101	.0104	125	5	-30	2	2	175	2100	.12	.0118	
100	10	-20	1.4	1	350	1500	.224	.0379	.0127	125	5	-30	2	2	175	2200	.12	.0085	
100	10	-20	1.4	1	350	2200	.216	.0162	.0217	125	1.8	-30	2	2	175	2300	.12	.0059	
100	10	-20	1.4	1	350	2350	.212	.0097	.0237	125	1.8	-30	2	2	175	2400	.12	.0029	
100	10	-20	2	2	175	0	.117	.0255	.0007	125	12	-30	2	2	175	1500	.11	.0190	
100	10	-20	2	2	175	1500	.118	.0150	.0015	125	13.5	-30	4	2	180	1500	.14	.0215	
100	10	-20	2	2	175	1550	.117	.0130	.0026	125	14.5	-30	6	2	180	1500	.15	.0234	
100	10	-20	2	2	175	1600	.117	.0122	.0027	125	7	-30	2	2	175	2450	.11	.0010	
100	10	-20	2	2	175	1650	.116	.0104	.0034	125	8	-30	4	2	180	2450	.14	.0031	
100	10	-20	2	2	175	1700	.116	.0100	.0036	125	10	-30	6	2	180	2450	.15	.0048	
100	10	-20	2	2	175	1750	.115	.0088	.0040	125	5	-30	2	3	195	1500	.12	.0204	
100	10	-20	2	2	175	1800	.115	.0069	.0057	125	10	-30	2	3	200	1500	.12	.0209	
100	10	-20	2	2	175	1850	.114	.0055	.0055	125	5	-30	0	1	330	1500	.15	.0324	
100	10	-20	2	2	175	1900	.115	.0038	.0059	125	5	-30	2	2	175	1500	.12	.0200	
100	10	-20	2	2	175	1950	.115	.0022	.0071	125	1.8	-30	-2	1	325	1500	.13	.0281	
100	10	-20	2	2	175	2000	.114	.0004	.0076	125	1.8	-50	-2	1	310	2450	.12	.0091	
100	10	-20	2	2	175	2050	.113	-.0017	.0083	150	1.8	-30	0	2	175	1700	.10	.0196	
100	10	-20	2	2	175	2100	.113	-.0030	.0087	150	1.8	-35	0	2	175	2100	.10	.0146	
100	10	-20	2	2	175	2150	.113	-.0049	.0096	150	1.8	-35	0	2	175	2200	.10	.0130	
100	10	-20	2	2	175	2200	.113	-.0074	.0105	150	10	-30	2	2	180	1500	.11	.0203	
100	10	-20	2	2	175	2250	.112	-.0089	.0117	150	7	-30	2	2	180	2300	.12	.0117	
100	10	-20	2	2	175	2300	.110	-.0119	.0128	150	7	-30	2	2	180	2400	.12	.0097	
										150	6	-30	2	2	180	2500	.12	.0078	↓

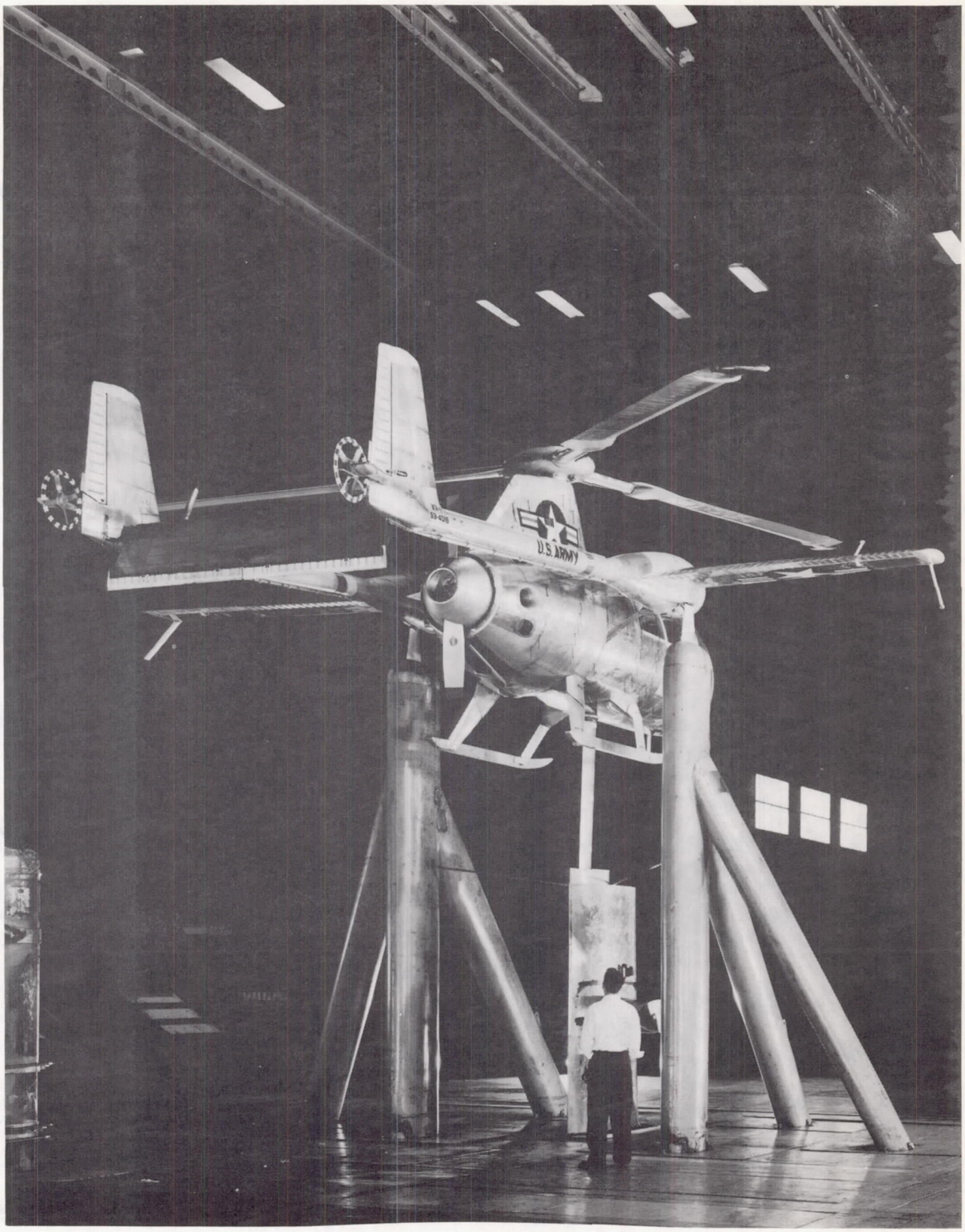
[1]Configuration 1 - autogiro-type flight
Configuration 2 - airplane-type flight
Configuration 3 - same as 2, but rotor rpm governor inoperative
[2]Aircraft free to float



A-19328

(a) Front view.

Figure 1.- Photograph of the XV-1 convertiplane mounted in the Ames 40- by 80-foot wind tunnel.



A-19327

(b) Three-quarter rear view.

Figure 1.- Concluded.

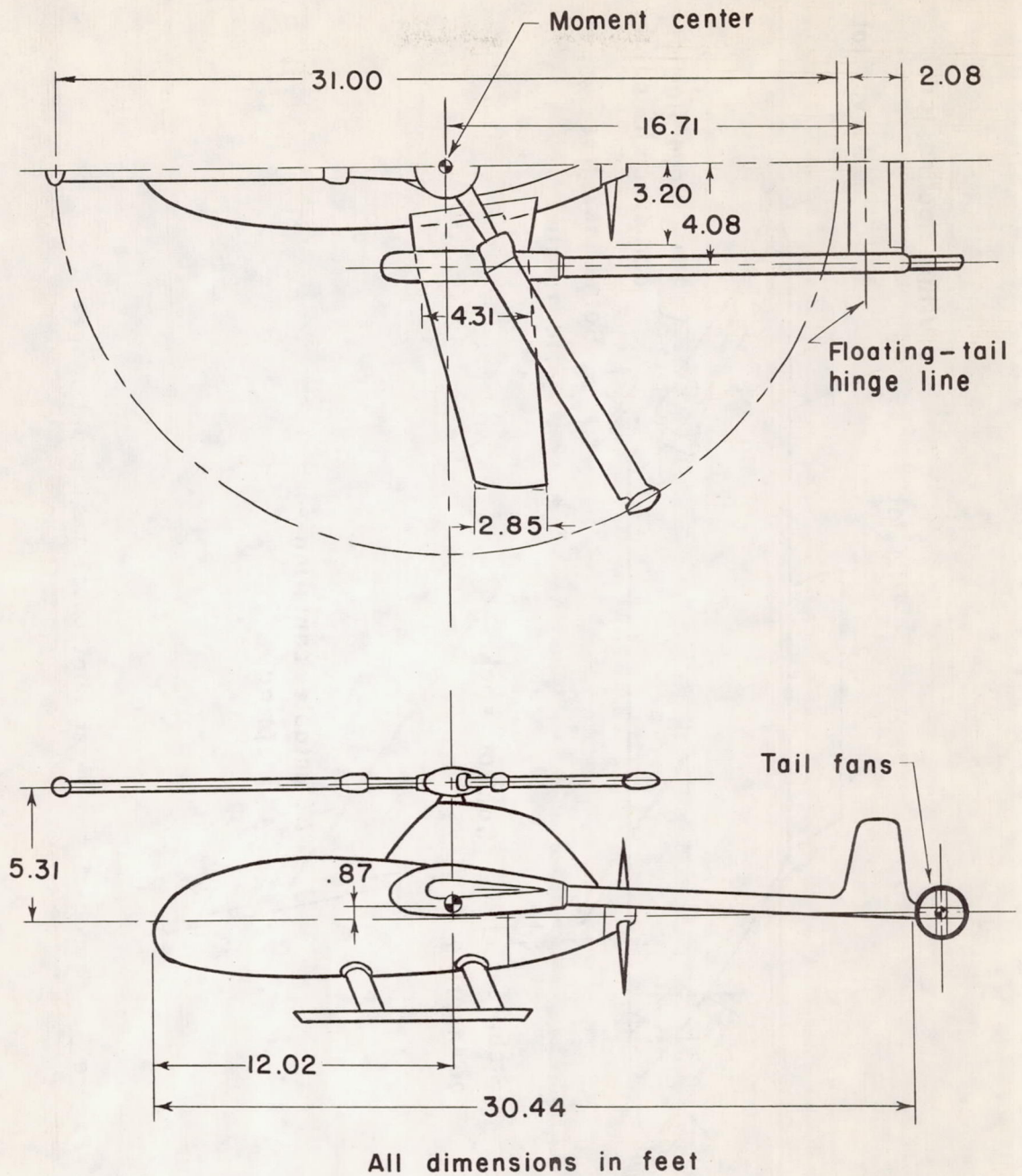


Figure 2.- General arrangement of the XV-1 convertiplane.

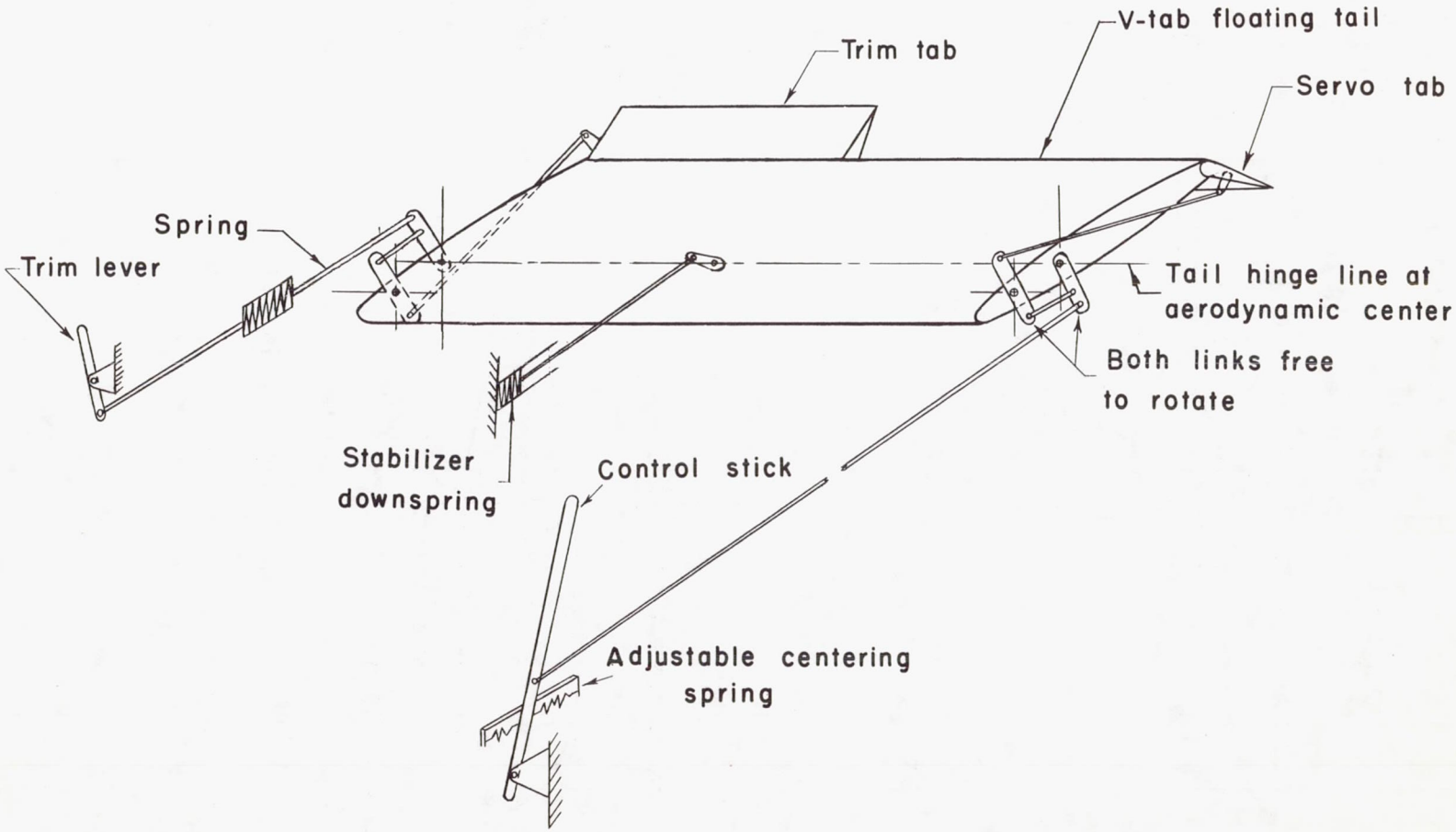
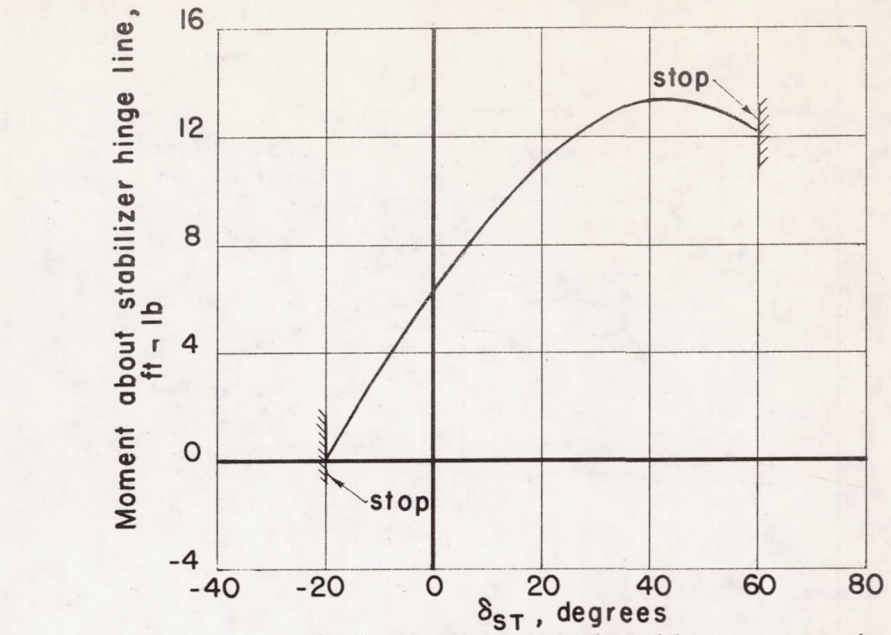
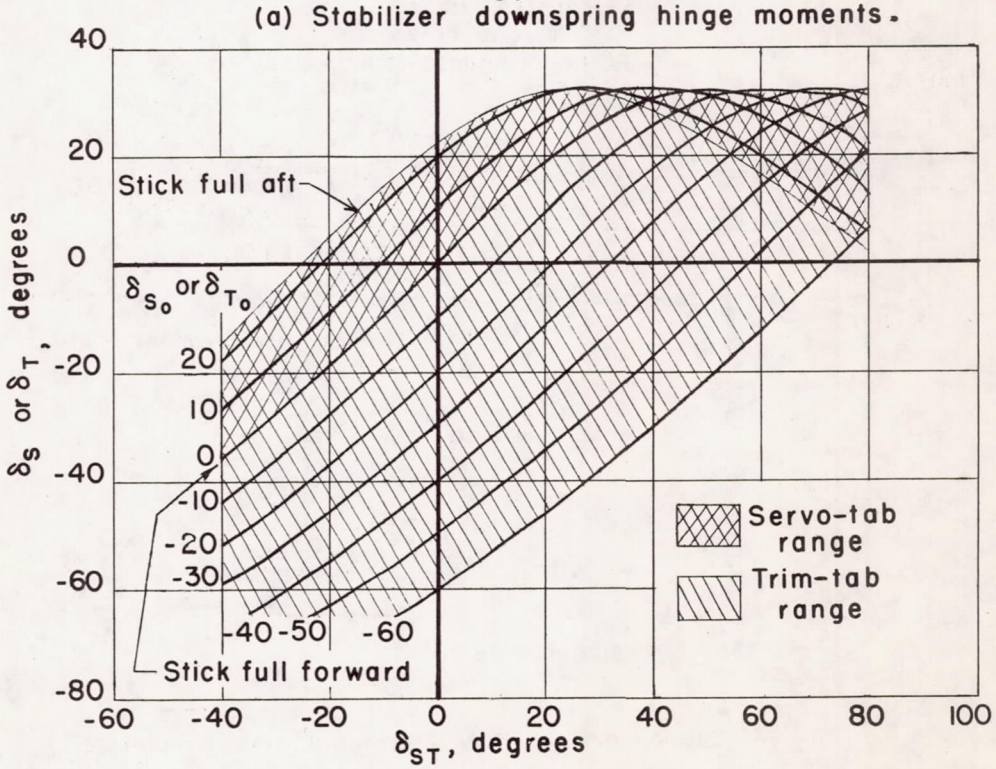


Figure 3.- Sketch of the V-tab horizontal tail and linkages.



(a) Stabilizer downspring hinge moments.



(b) Linkage characteristics.

Figure 4.- Variation of downspring hinge moment and tab angle with stabilizer angle.

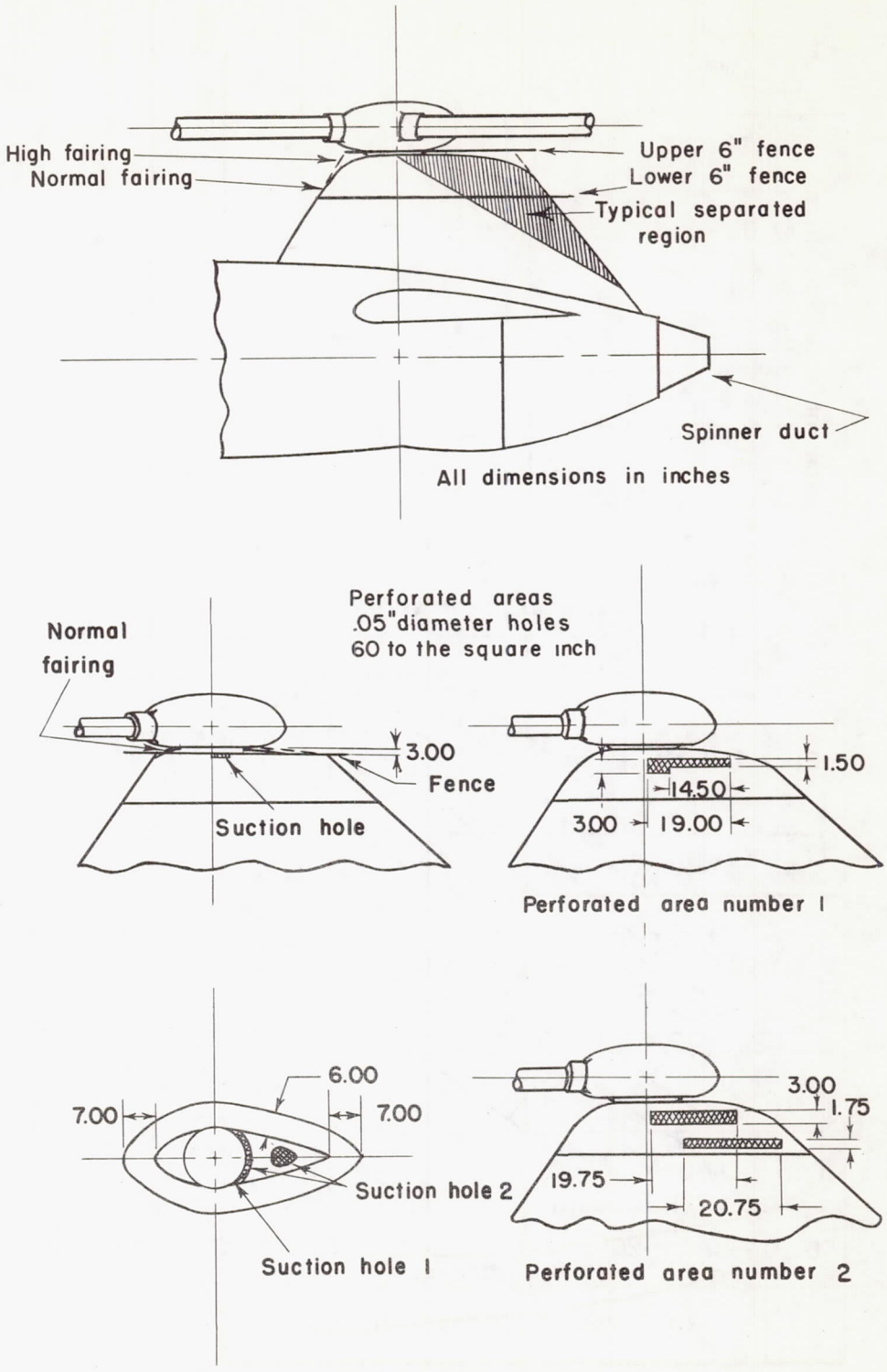


Figure 5.- Pylon fence and suction configurations.

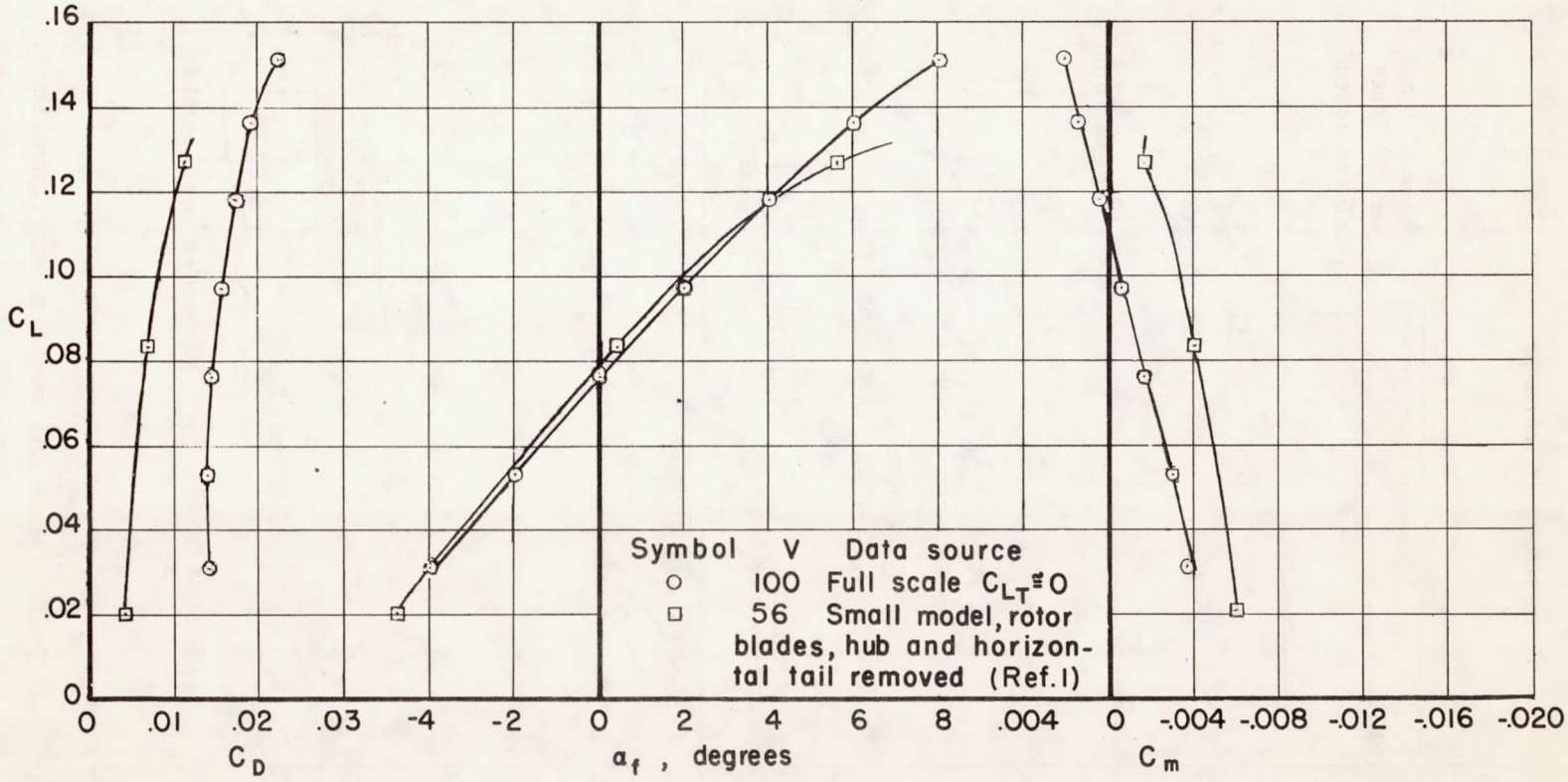
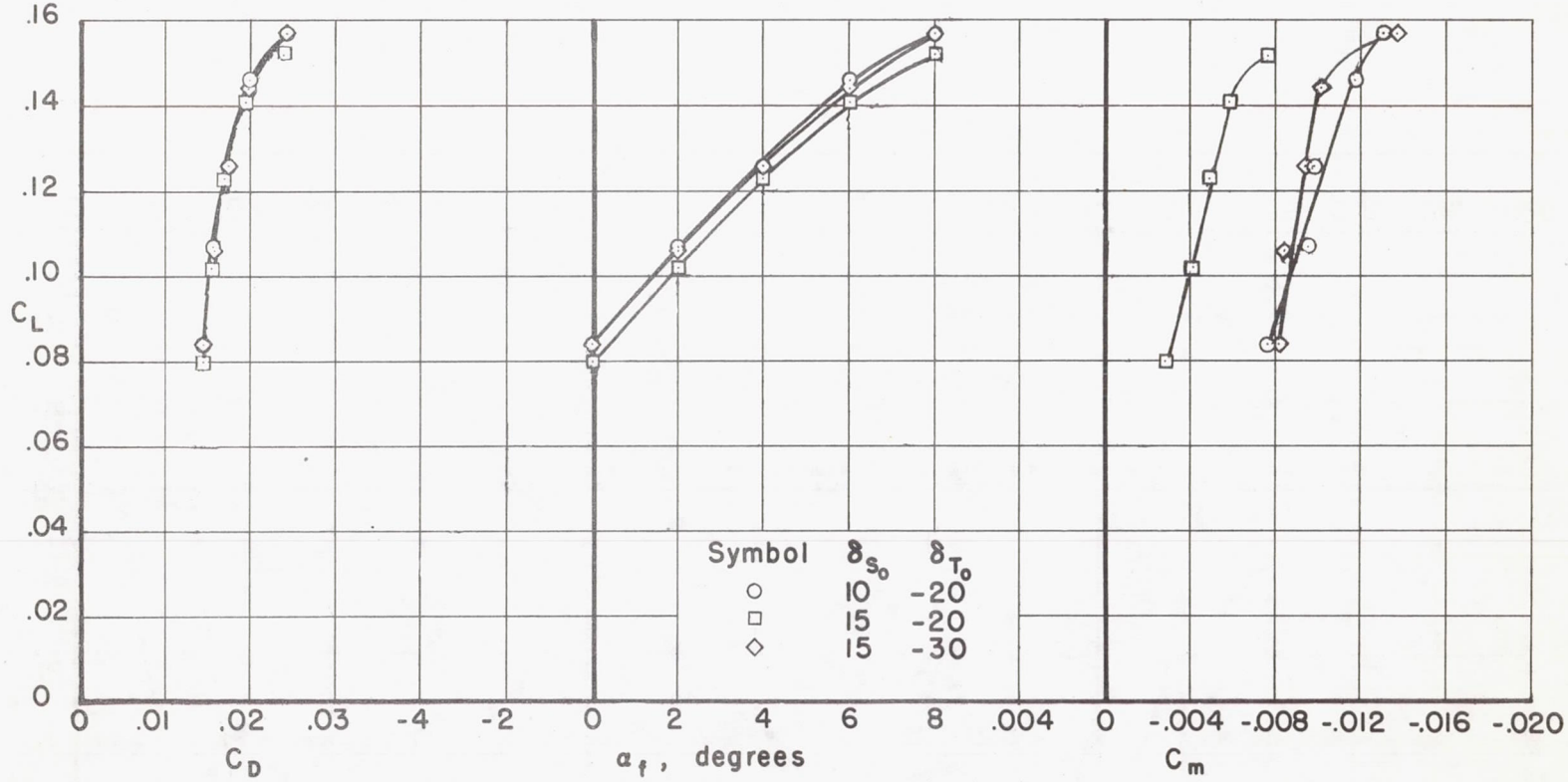
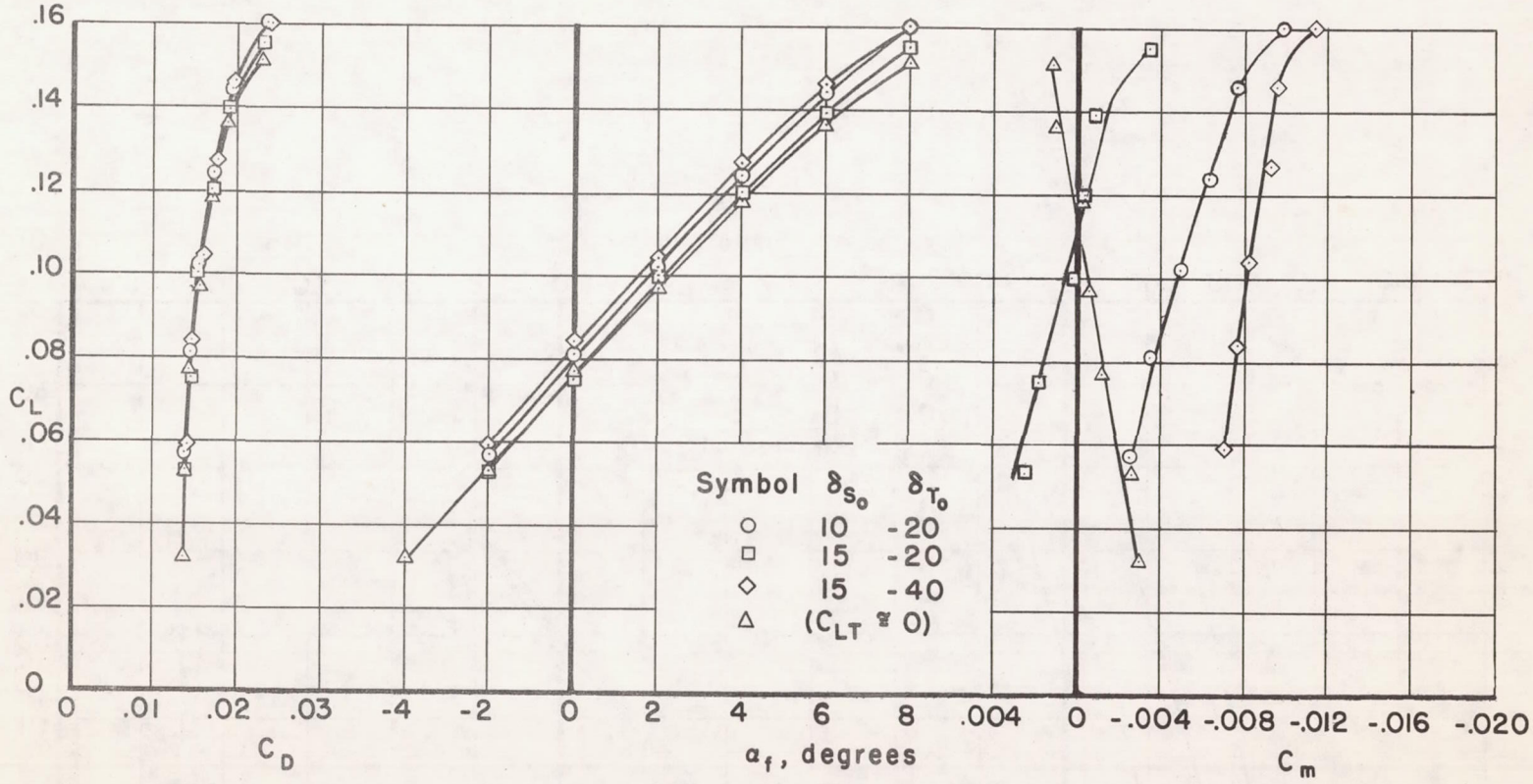


Figure 6.- Longitudinal characteristics with the rotor blades and propeller removed and zero tail load.



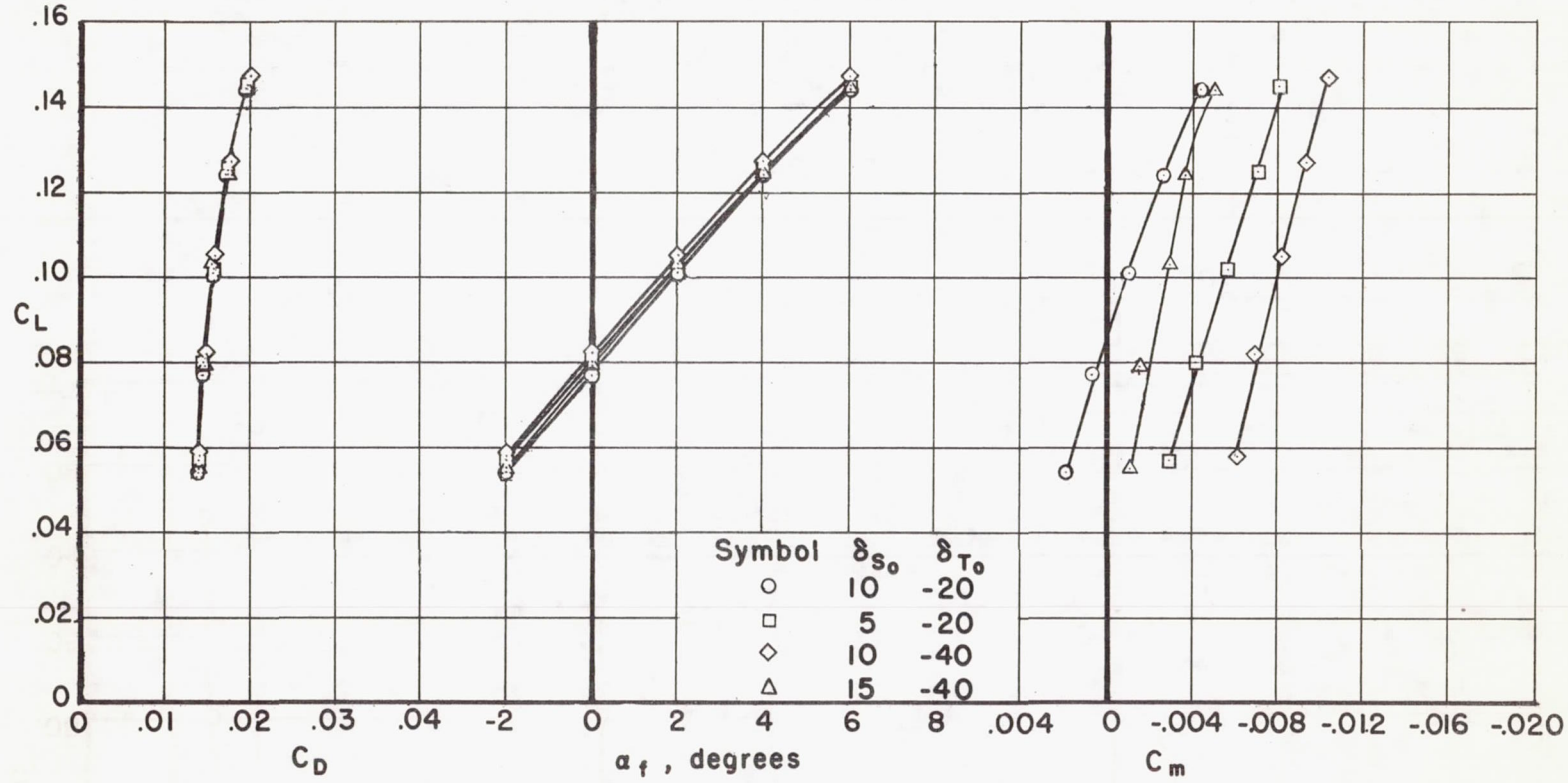
(a) V = 75 knots

Figure 7.- Longitudinal characteristics with the rotor blades and propeller removed.



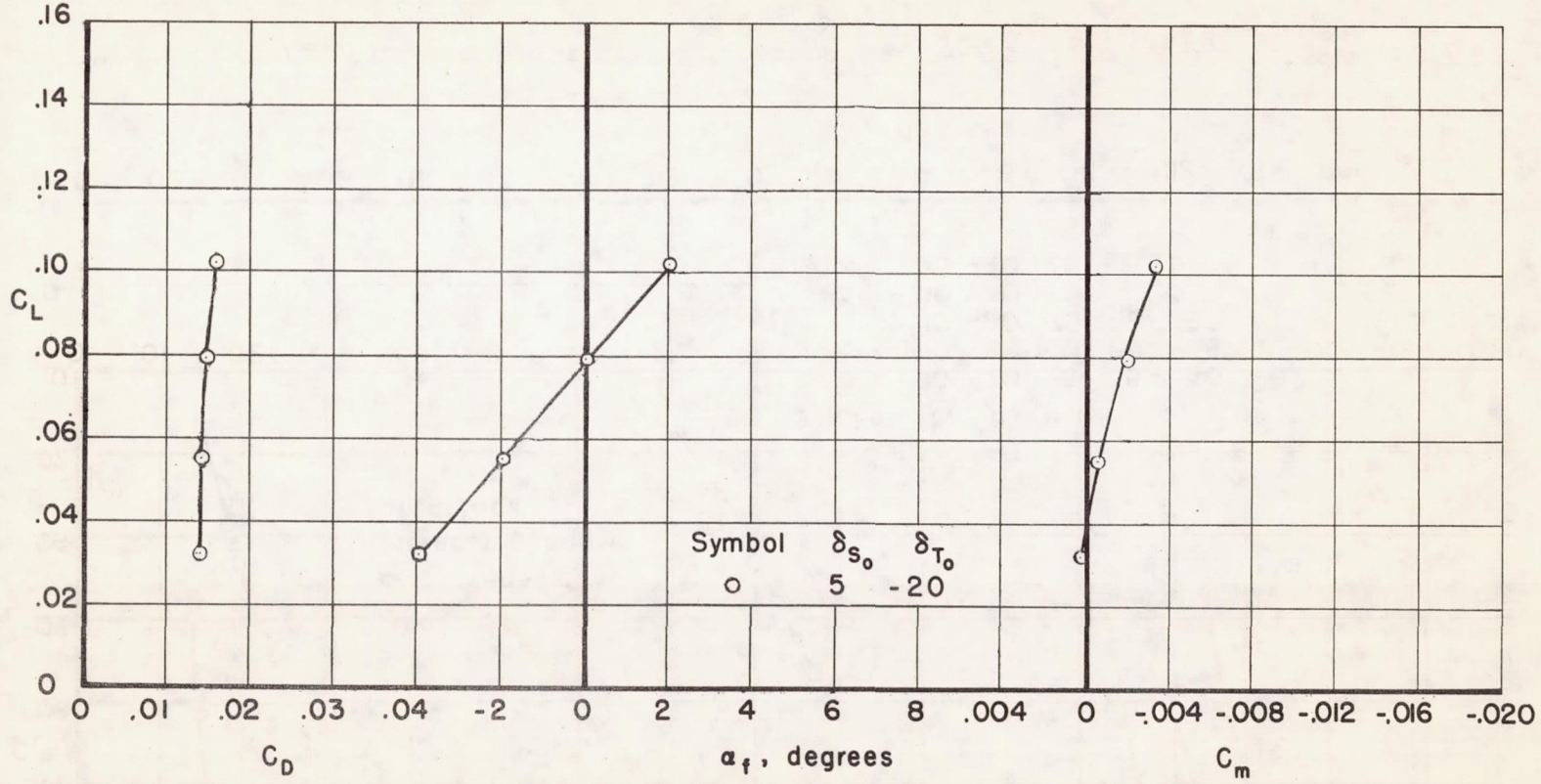
(b) V = 100 knots

Figure 7.- Continued.



(c) V = 125 knots

Figure 7.- Continued.



(d) V = 150 knots

Figure 7.- Concluded.

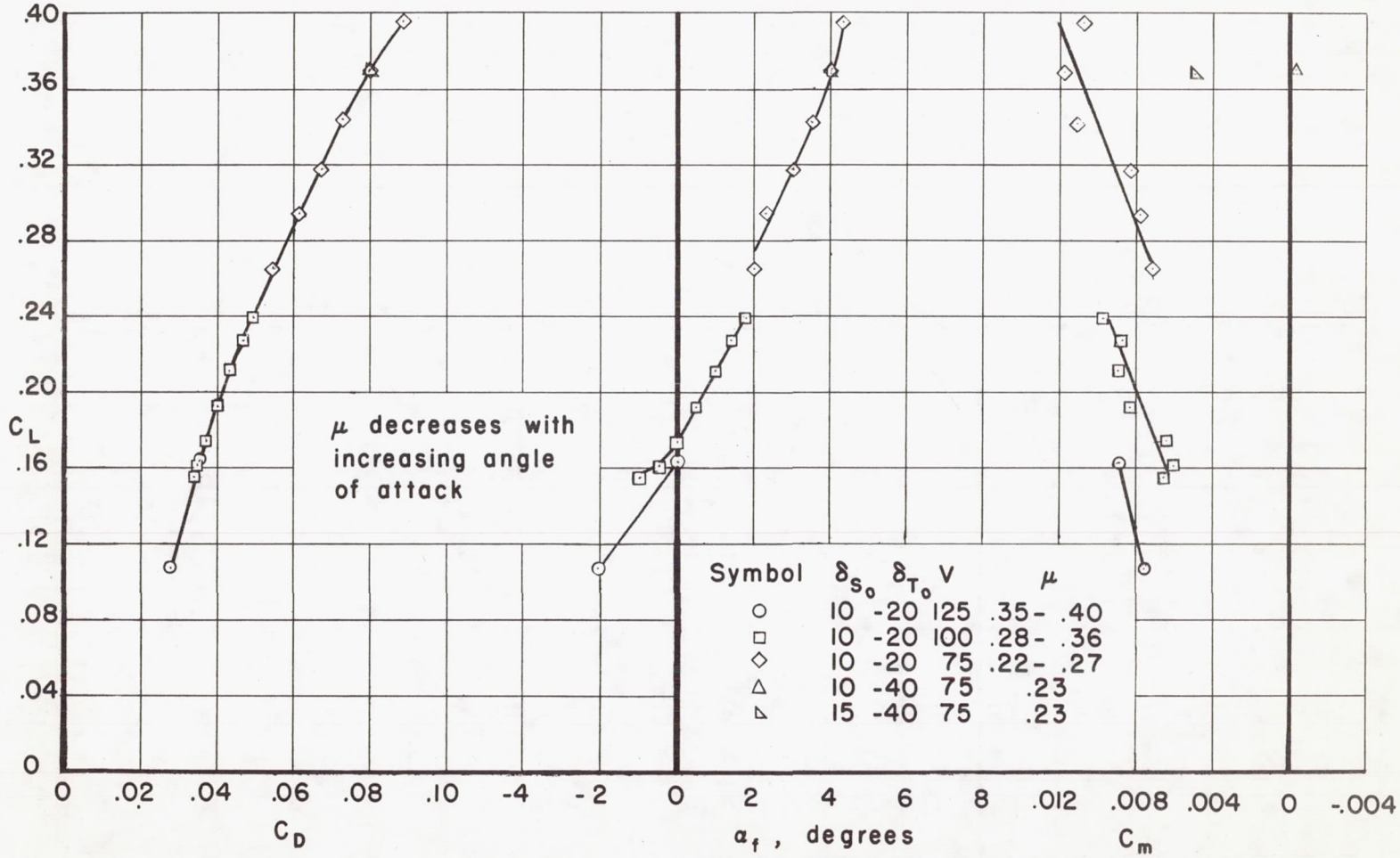


Figure 8.- Longitudinal characteristics of the autogiro-type flight configuration; propeller removed.

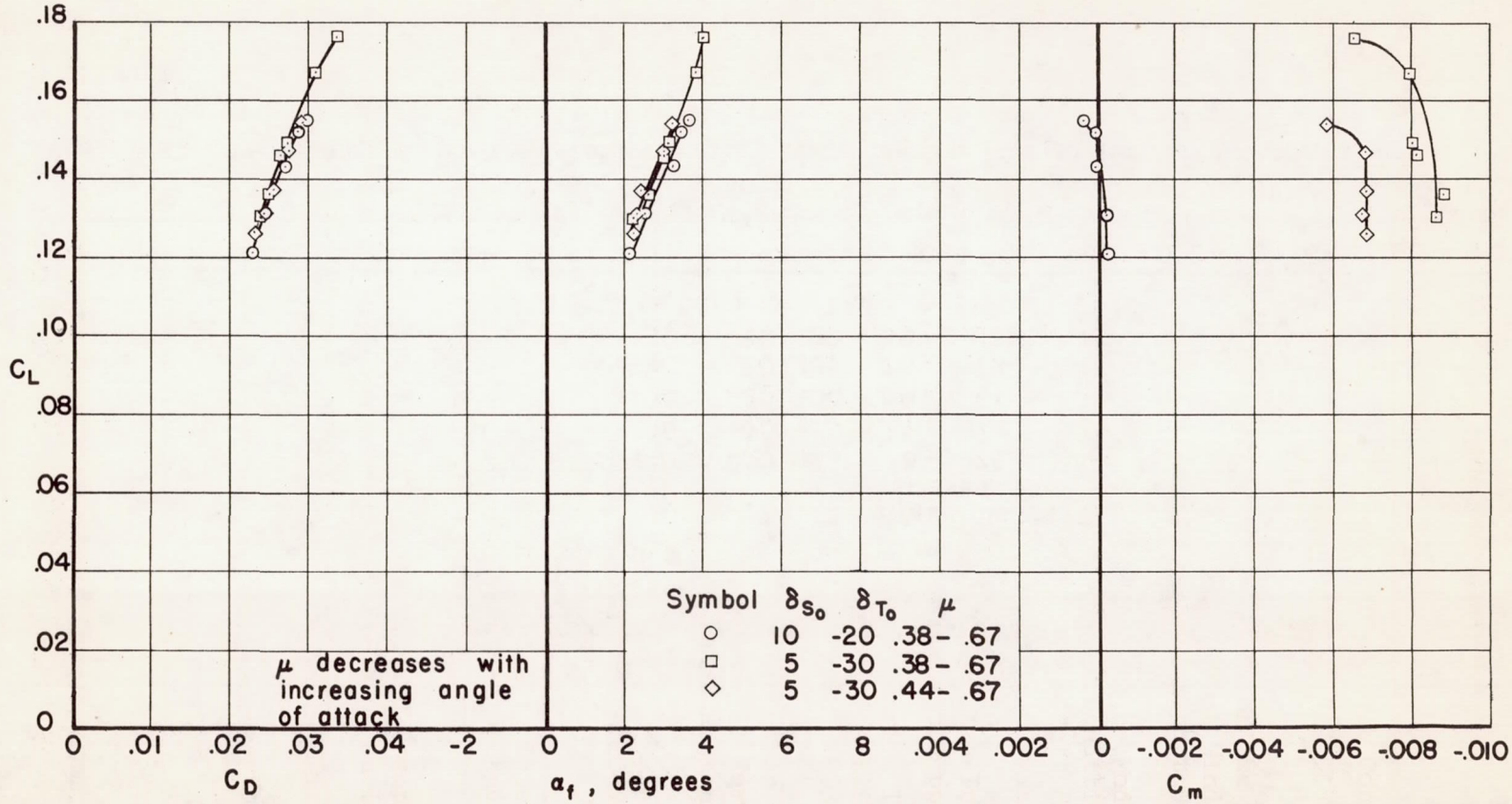


Figure 9.- Longitudinal characteristics of the airplane-type flight configuration with the rotor rpm governor inoperative; propeller removed, V = 113 knots.

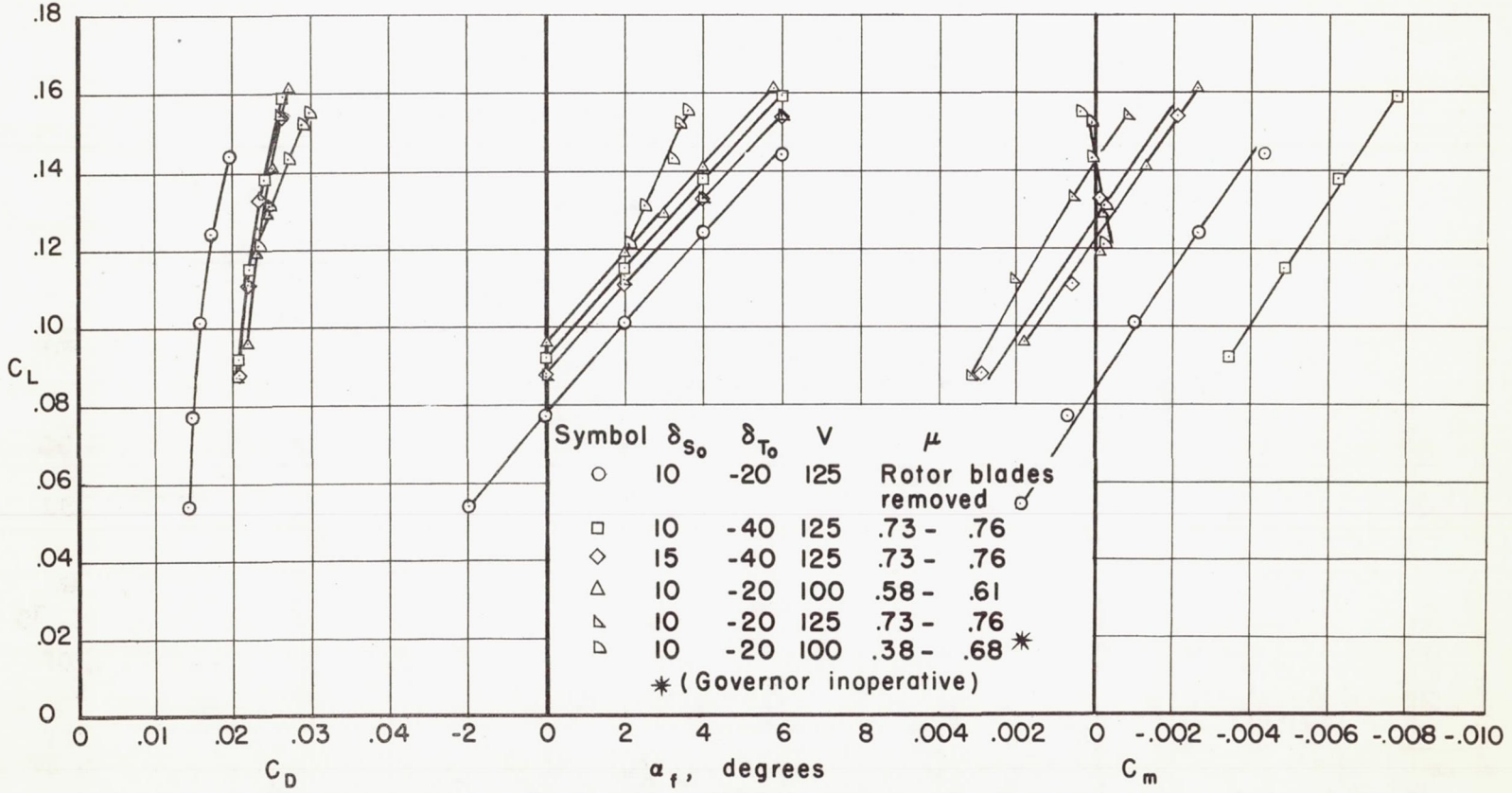


Figure 10.- Longitudinal characteristics of the airplane-type flight configuration; propeller removed.

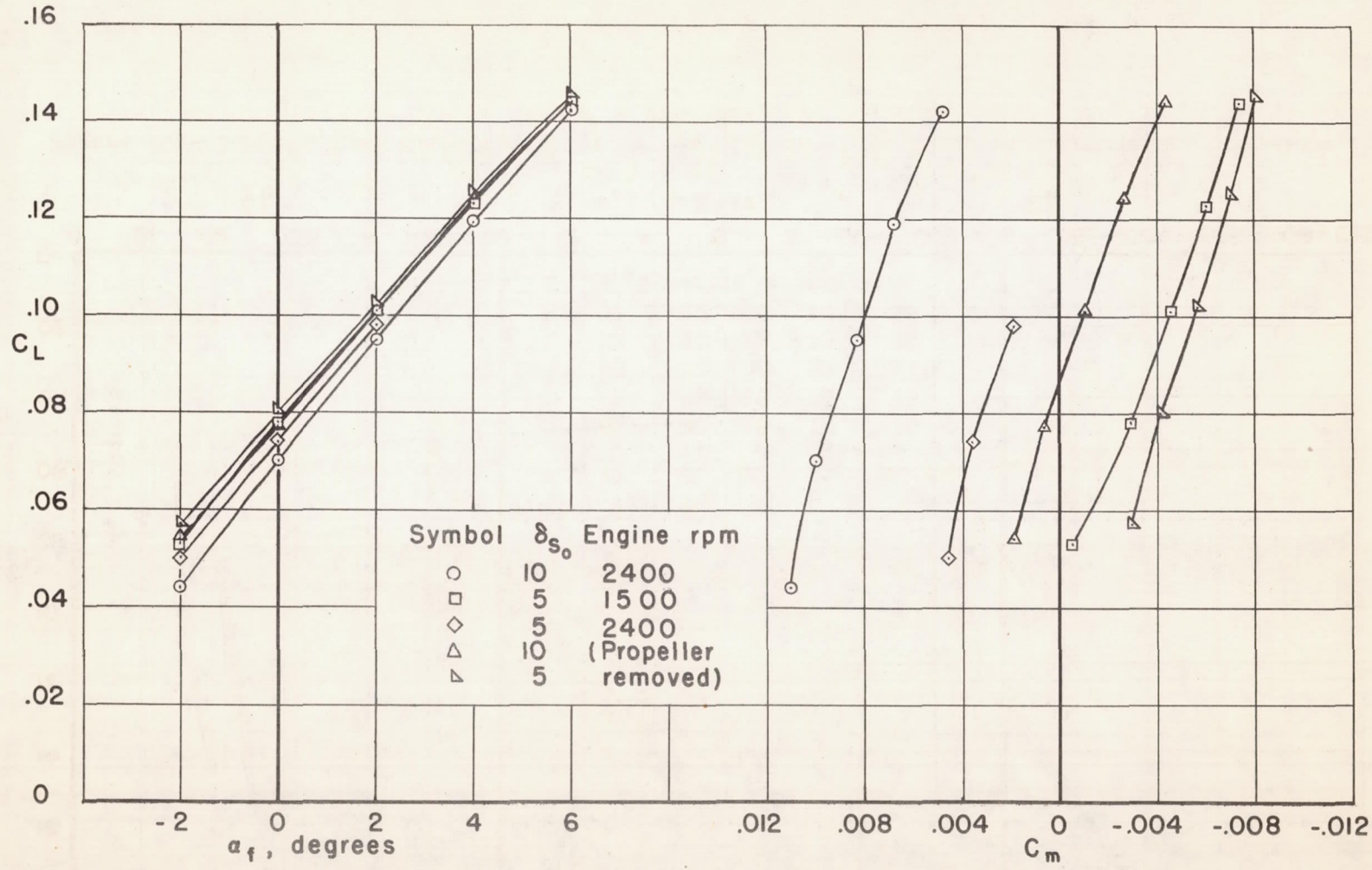
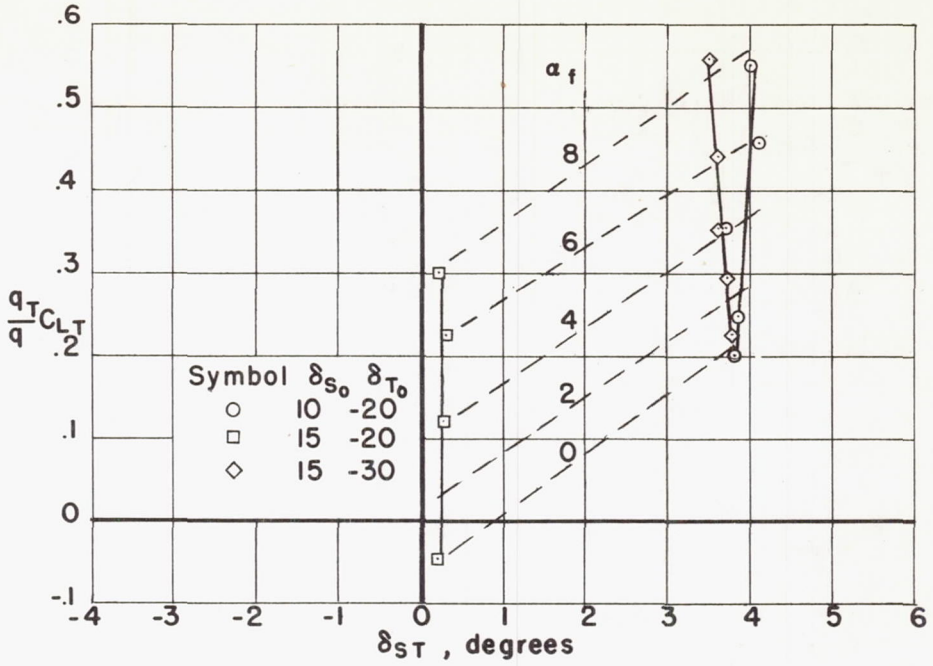
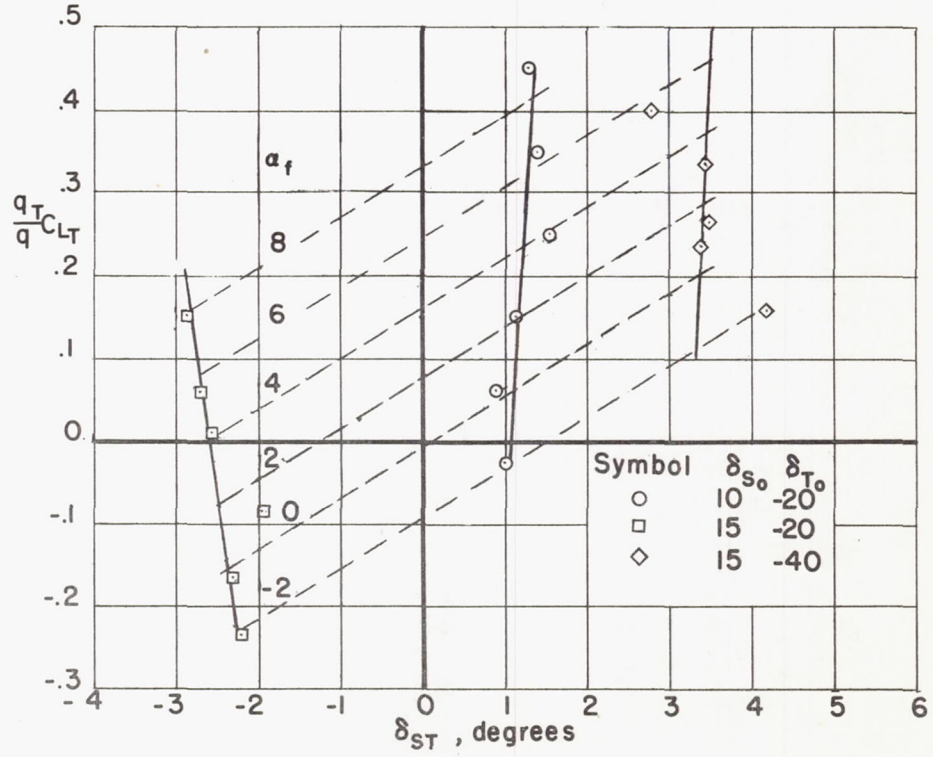


Figure 11.- Effect of power on the longitudinal characteristics; rotor blades removed, V = 125 knots, $\delta_{T_o} = -20^\circ$.

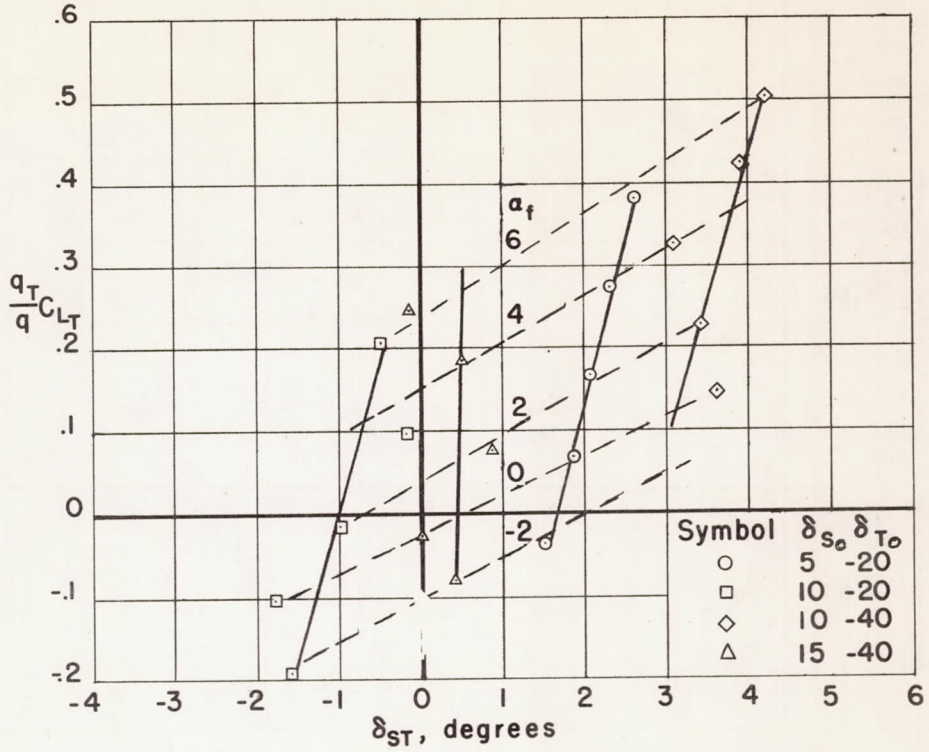


(a) V = 75 knots

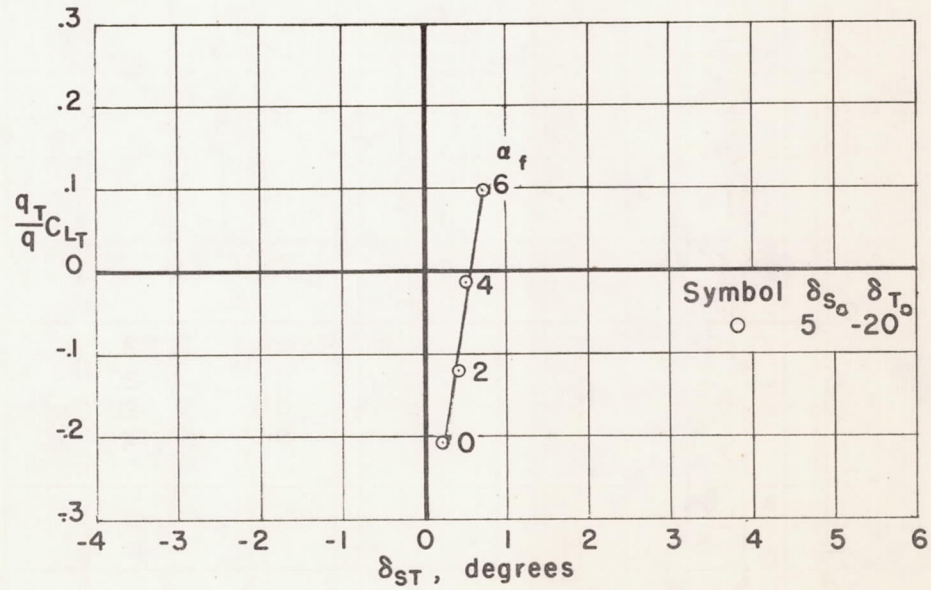


(b) V = 100 knots

Figure 12.- Aerodynamic characteristics of the V-tab horizontal tail.



(c) V = 125 knots



(d) V = 150 knots

Figure 12.- Concluded.

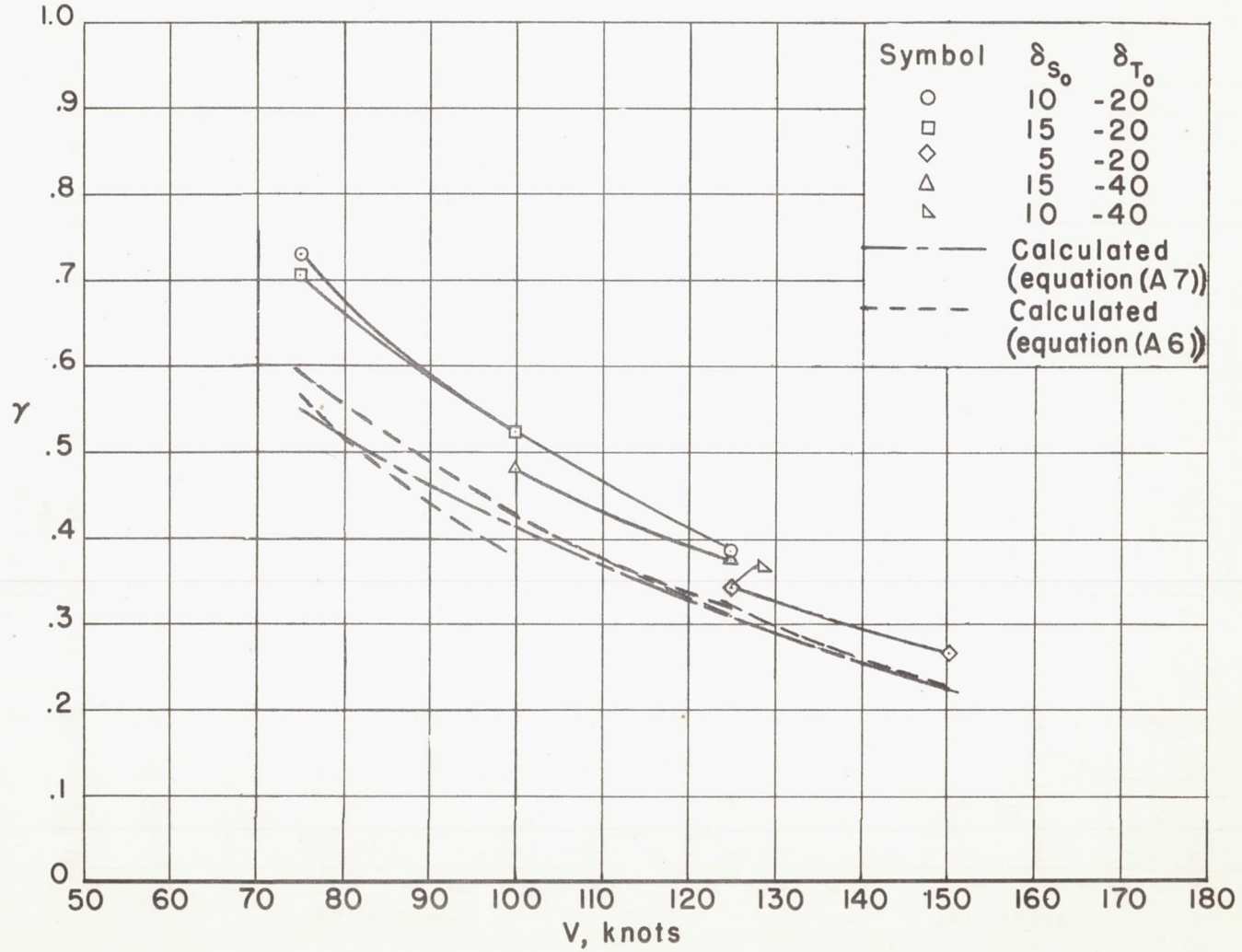
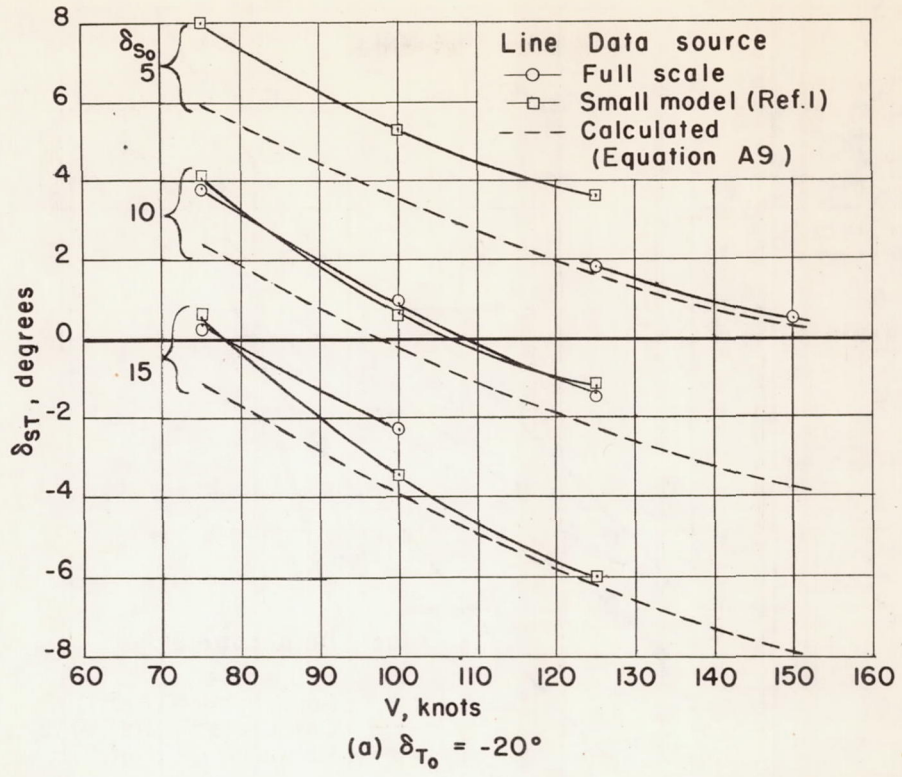


Figure 13.- Comparison of the calculated and experimental trim-tab deflection ratios.



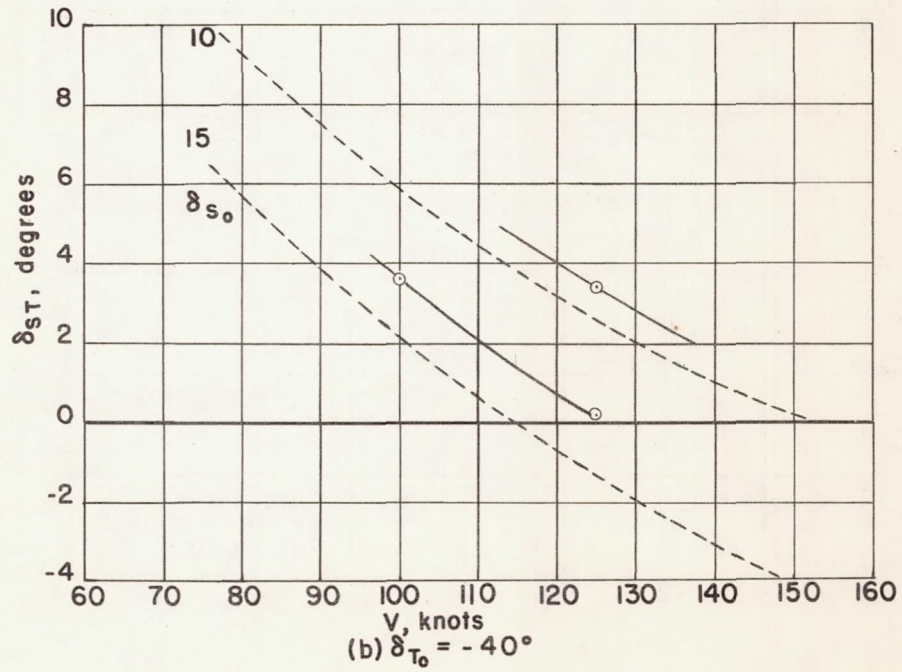
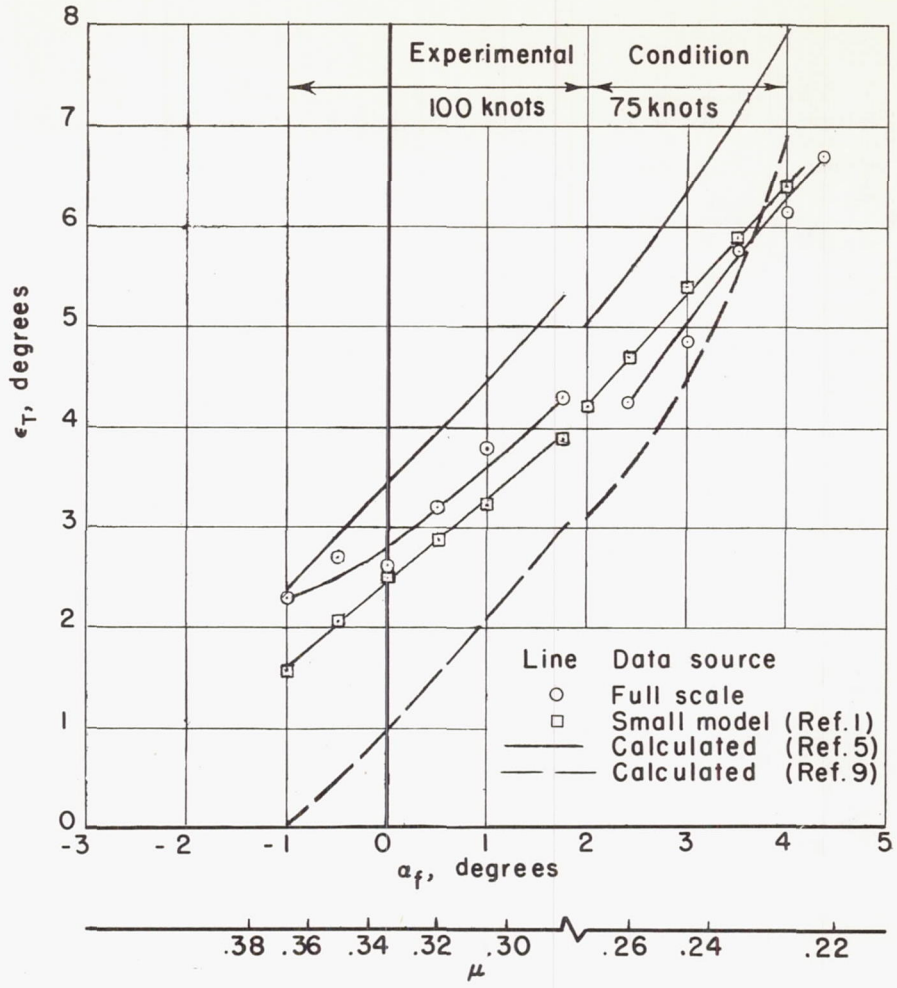
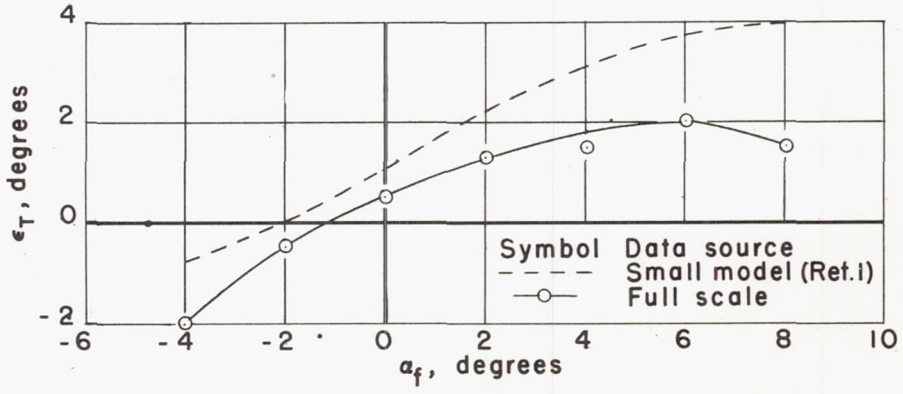


Figure 14.- Variation of stabilizer incidence angle with airspeed for various servo-tab and trim-tab setting combinations.

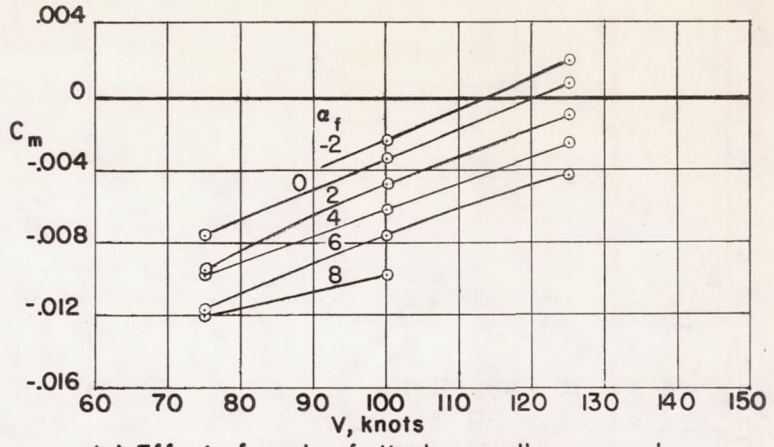


(a) Autogiro-type flight configuration.

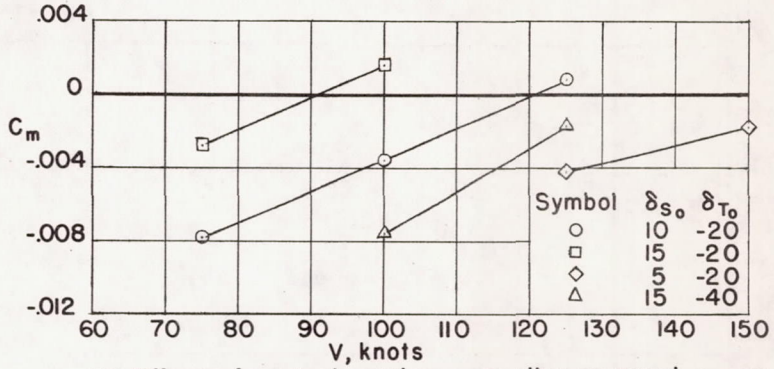


(b) Rotor blades removed.

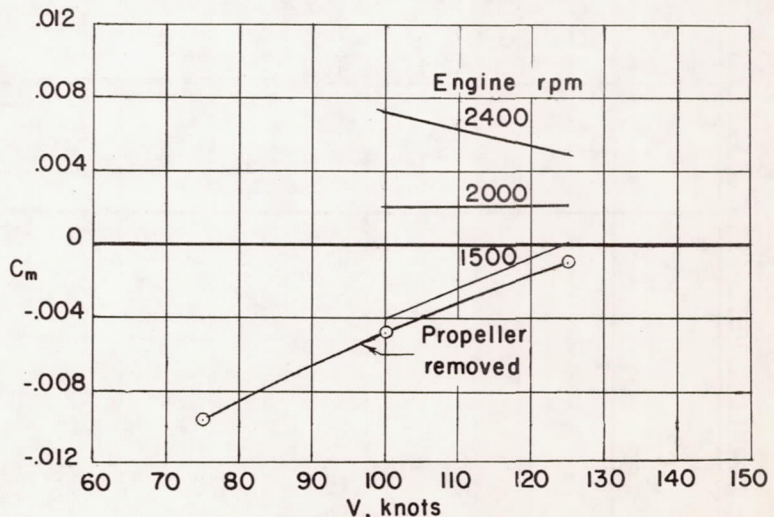
Figure 15.- Comparison of full-scale, small-model, and theoretical downwash angles at the tail.



(a) Effect of angle of attack, propeller removed, $\delta_{S_o}=10°$ $\delta_{T_o}=-20°$.

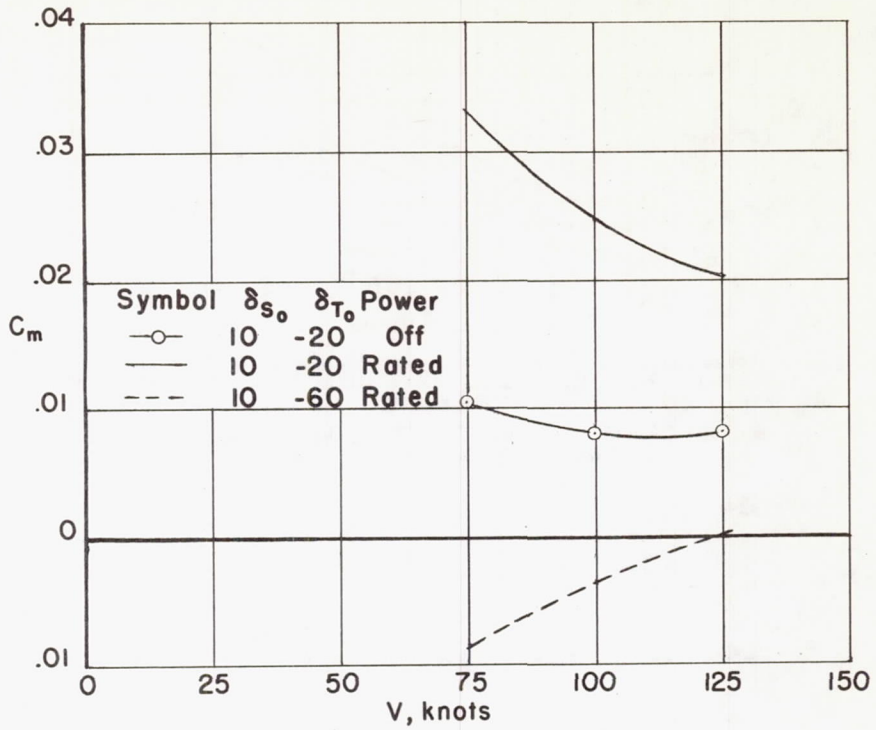


(b) Effect of control setting, propeller removed, $\alpha_f=0°$.

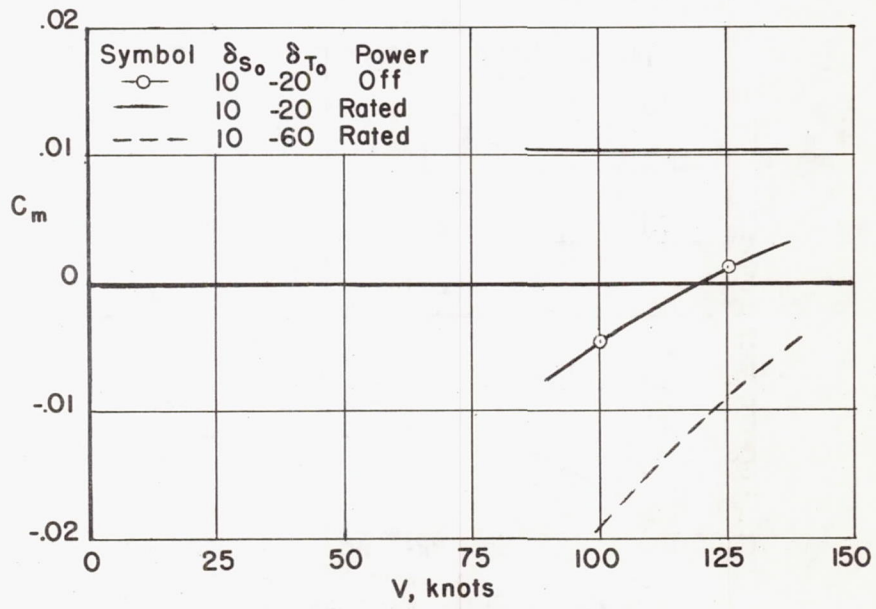


(c) Effect of propeller operation, $\alpha_f=2°$, $\delta_{S_o}=10°$, $\delta_{T_o}=-20°$.

Figure 16.- Pitching moment versus airspeed characteristics; rotor blades removed.

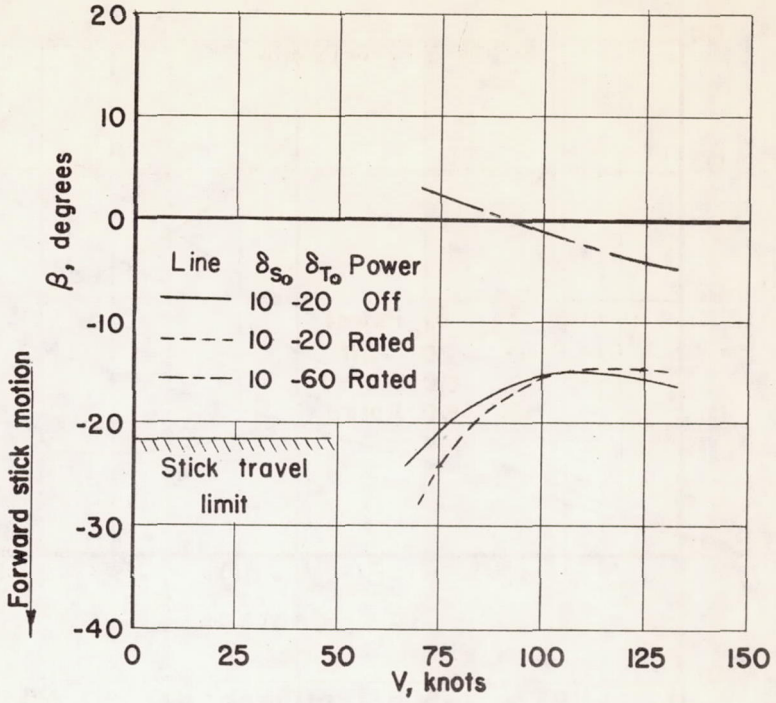


(a) Autogiro-type flight.

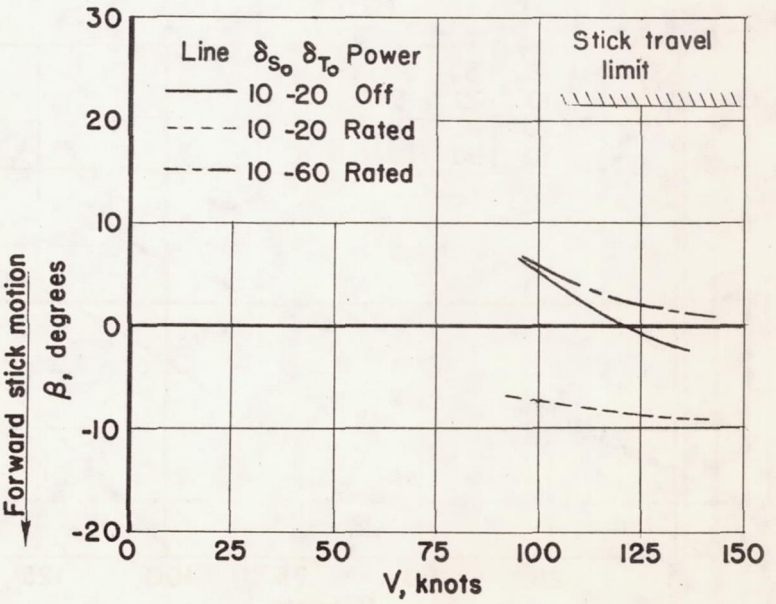


(b) Airplane-type flight.

Figure 17.- Pitching moments at the lift coefficient for level flight and corresponding stick position for trim.

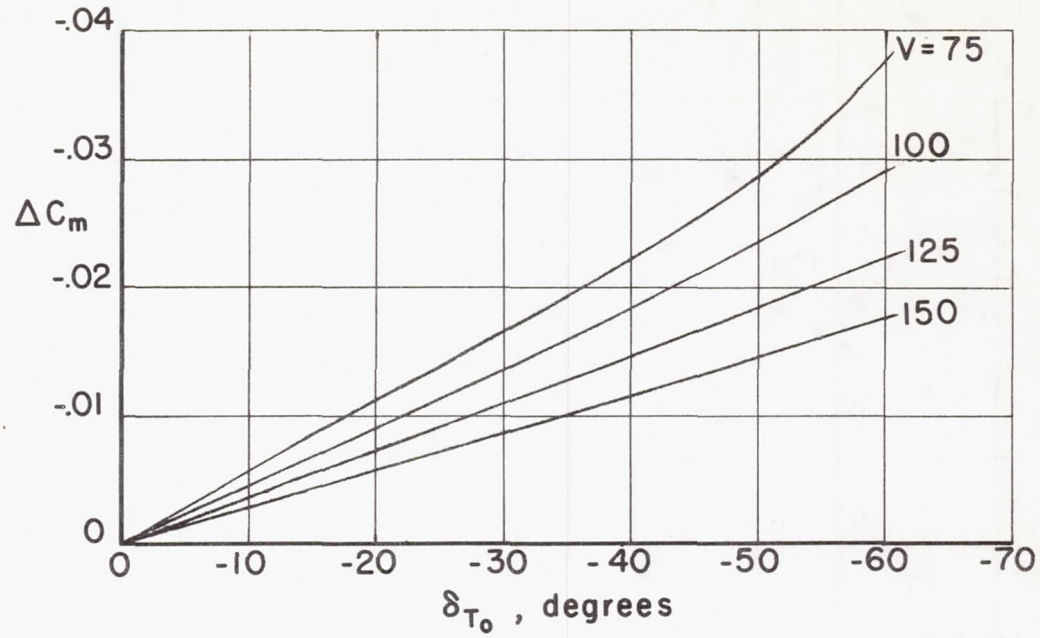


(c) Autogiro-type flight.

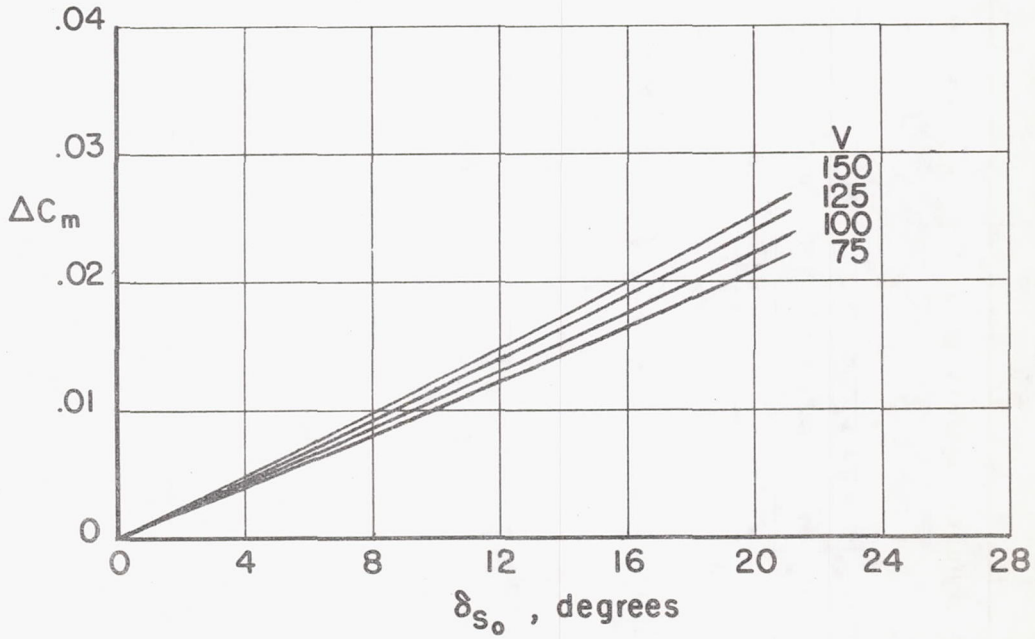


(d) Airplane-type flight.

Figure 17.- Concluded.



(a) Trim-tab effectiveness, $\delta_{S_o} = 0$.



(b) Servo-tab effectiveness, $\delta_{T_o} = 0$.

Figure 18.- Calculated longitudinal-control effectiveness; propeller removed.

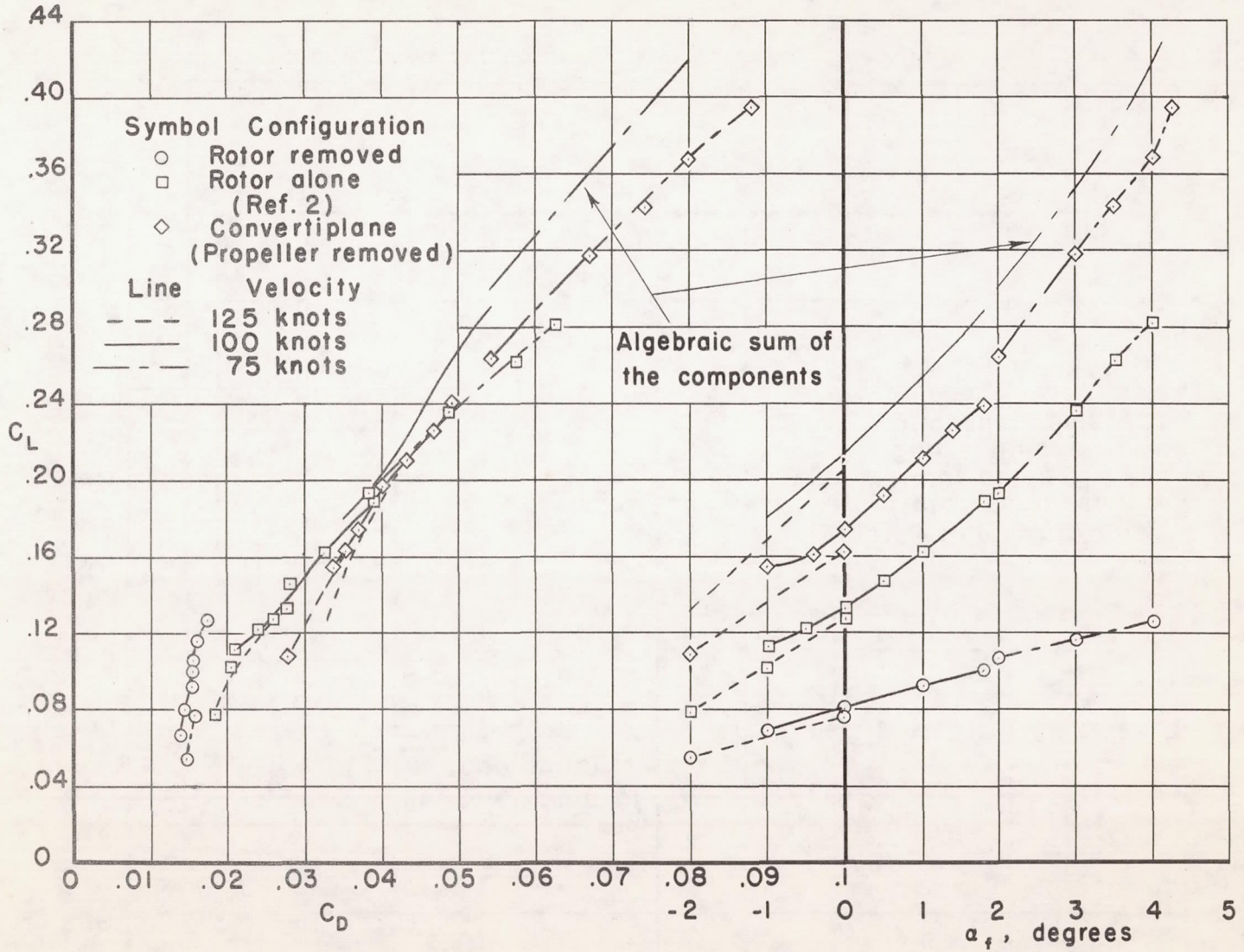


Figure 19.- Lift and drag of the convertiplane and its components in the autogiro-type flight configuration; propeller removed, $\delta_{S_O} = 10^\circ$, $\delta_{T_O} = -20^\circ$.

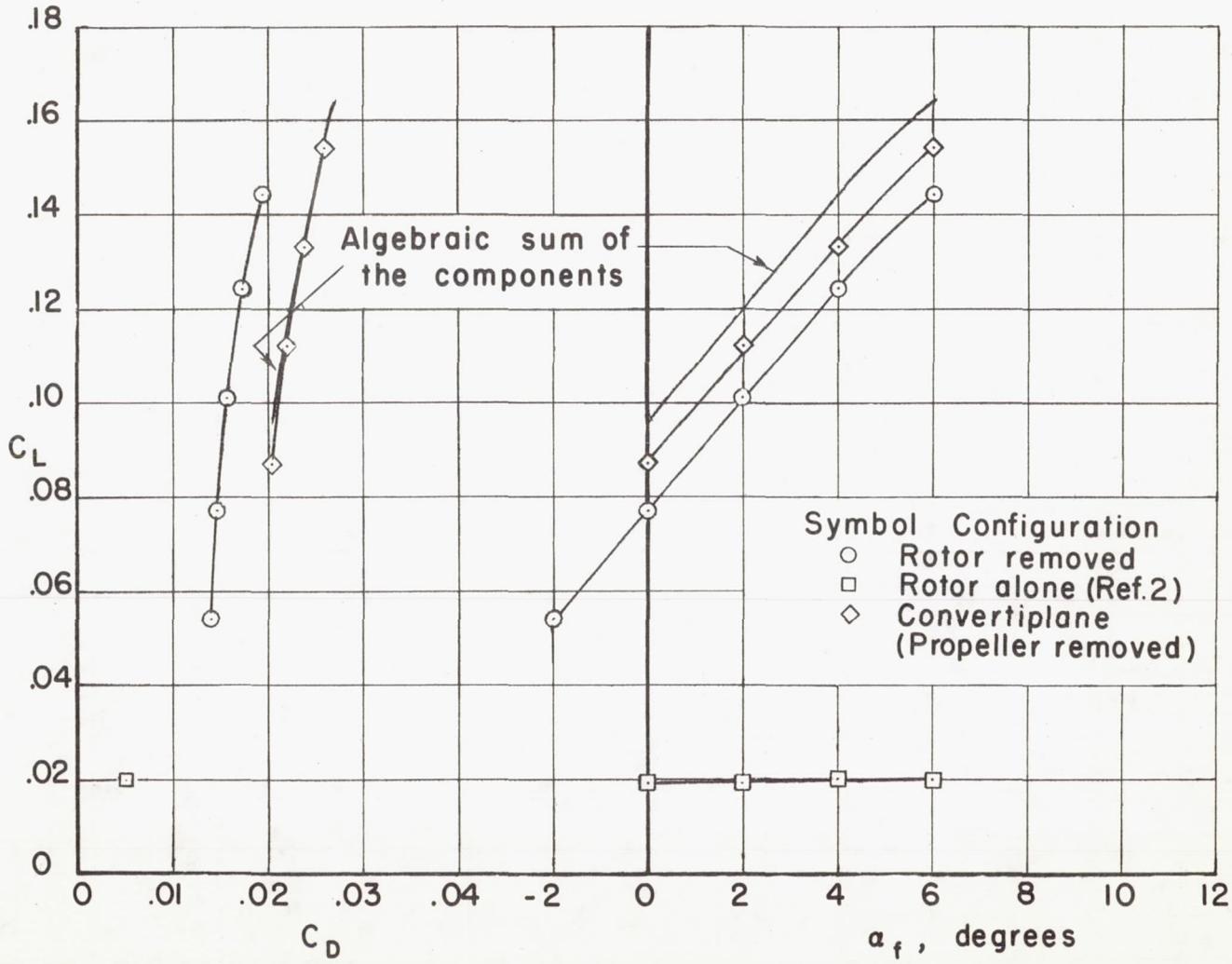


Figure 20.- Lift and drag of the convertiplane and its components in the airplane-type flight configuration; propeller removed, $\delta_{S_O} = 10^\circ$, $\delta_{T_O} = -20^\circ$, V = 125 knots.

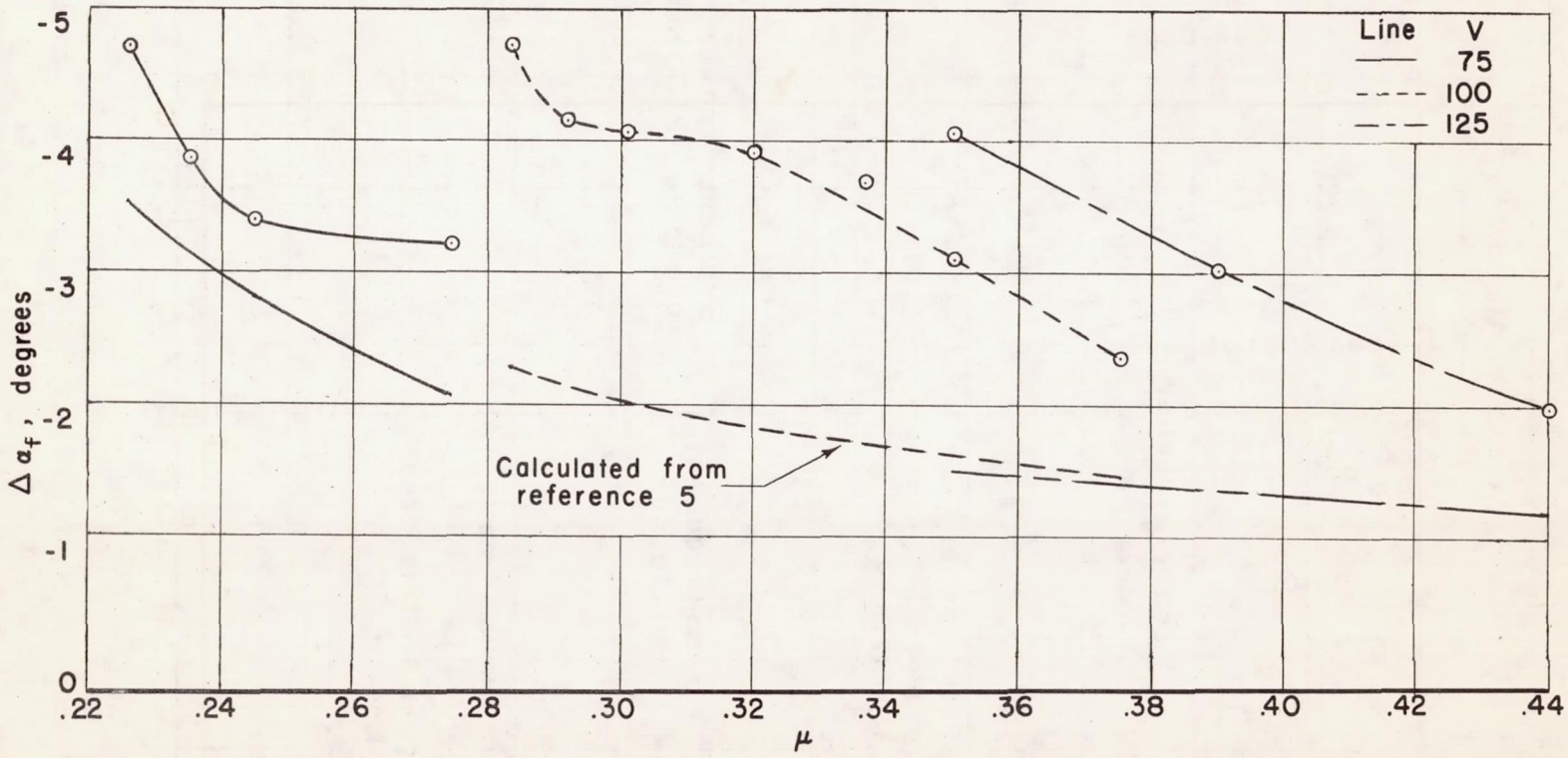


Figure 21.- Change in angle of attack of the wing due to the rotor downwash required to fully account for the loss in lift of the combination.

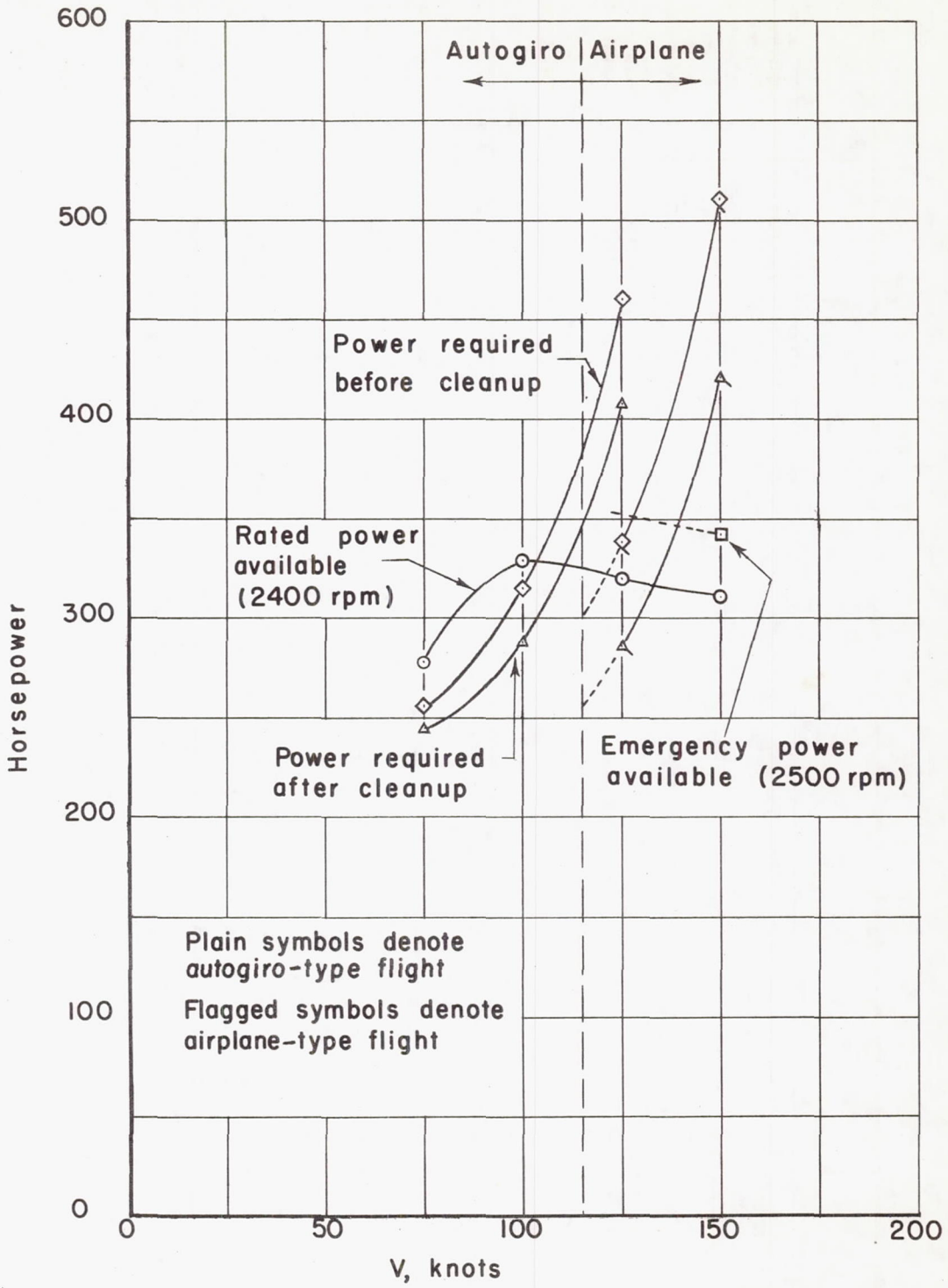


Figure 22.- Thrust horsepower available and required at sea level; gross weight = 5,000 pounds.